BRL MR 2744

BRL

MEMORANDUM REPORT NO. 2744

PROCEDURE FOR THE REDUCTION OF IR SCANNER DATA

J. Terrence Klopcic
John E. Kammerer

April 1977

USA ARMAMENT RESEARCH AND DEVELOPMENT COMMAND
USA BALLISTIC RESEARCH LABORATORY
ABERDEEN PROVING GROUND, MARYLAND

Destroy this report when it is no longer needed.
Do not return it to the originator.

Secondary distribution of this report by originating or sponsoring activity is prohibited.

Additional copies of this report may be obtained from the National Technical Information Service, U.S. Department of Commerce, Springfield, Virginia 22151.

The findings in this report are not to be construed as an official Department of the Army position, unless so designated by other authorized documents.

UNCLASSIFIED

SECURITY CLASSIFICATION OF THIS PAGE (When Data Entered)

REPORT DOCUMENTATION PAGE	READ INSTRUCTIONS BEFORE COMPLETING FORM
1. REPORT NUMBER: BRL MEMORANDUM REPORT NO. 2744	2. GOVT ACCESSION NO. / 3. RECIPIENT'S CATALOG NUMBER
4. TITLE (and Subtitle): PROCEDURE FOR THE REDUCTION OF IR SCANNER DATA	5. TYPE OF REPORT & PERIOD COVERED: Final
	6. PERFORMING ORG. REPORT NUMBER
7. AUTHOR(s): J. Terrence Klopcic John E. Kammerer	8. CONTRACT OR GRANT NUMBER(s)
9. PERFORMING ORGANIZATION NAME AND ADDRESS: Director USA Ballistic Research Laboratory Aberdeen Proving Ground, MD 21005	10. PROGRAM ELEMENT, PROJECT, TASK AREA & WORK UNIT NUMBERS: 1X363314D093
11. CONTROLLING OFFICE NAME AND ADDRESS: U.S. Army Materiel Development & Readiness Cmd 5001 Eisenhower Avenue Alexandria, VA 22333	12. REPORT DATE: APRIL 1977 13. NUMBER OF PAGES: 65
14. MONITORING AGENCY NAME & ADDRESS (if different from Controlling Office)	15. SECURITY CLASS. (of this report): UNCLASSIFIED 15a. DECLASSIFICATION/DOWNGRADING SCHEDULE

16. DISTRIBUTION STATEMENT (of this Report)

Approved for public release; distribution unlimited.

17. DISTRIBUTION STATEMENT (of the abstract entered in Block 20, if different from Report)

18. SUPPLEMENTARY NOTES

19. KEY WORDS (Continue on reverse side if necessary and identify by block number)

Infra-red Scanning Camera
Laser Beam Diagnostics
Data Reduction

20. ABSTRACT (Continue on reverse side if necessary and identify by block number)

The IR scanning camera is widely accepted as the best source of real-time laser beam diagnostics. It is also the most detailed, and hence requires an extensive amount of data reduction and interpretation to produce a tractable output.

The hardware, software and experience needed to process and display IR scanner data has been developed at BRL. The codes are production oriented, resulting in fast turn-around time with a minimum of tape handling.

DD FORM 1 JAN 73 1473 EDITION OF 1 NOV 65 IS OBSOLETE

UNCLASSIFIED

SECURITY CLASSIFICATION OF THIS PAGE (When Data Entered)

This report discusses the steps necessary in the IR scanner reduction process, including analytical bases for the smoothing and fitting portions of the scanner beam interpretation.

TABLE OF CONTENTS

LIST OF ILLUSTRATIONS

LIST OF ILLUSTRATIONS (CONTINUED)

I. INTRODUCTION

The continuing need for experimental damage and effects data for high energy laser interactions has resulted in a number of experimental programs within the three services. The outputs of these programs are compilations of burn-through or failure times as a function of such parameters as target material, target surface, shield thickness, air flow, and particularly beam size, shape and intensity. Unfortunately, the available laser devices which are powerful enough for realistic experiments permit only very imperfect control of beam size and average intensity, with no control over shape and the intensity of spikes. As a result, experimentalists are forced to set up their tests based on an anticipated average intensity, carefully diagnose the beam actually delivered, and interpret their results after the fact.

For continuous wave lasers, the best available technique for beam diagnostics involves the use of an infra-red (IR) scanning camera in conjunction with a real time beam power measurement (e.g. a chopper) and ball-calorimetry for absolute calibration. The scanning camera measures the diffuse reflection of the beam from a specular surface by imaging the (diffuse) beam reflection and sequentially scanning the image in a line-by-line fashion, similar to the scan of a black-and-white television camera. If a turning flat is used as the specular surface, the specularly reflected beam can be directed into the test target while the diffuse image is being IR-scanned; thus, a real-time measurement is made. The IR-scan results are only relative, since the shape of the beam is shown, but not the absolute intensities. However, absolute values are easily derived by integrating over the entire scanner picture, arriving at the scanner-relative total power, and normalizing to the real-time absolute total power measurement.

The results obtained from this normalization are absolute two-dimensional maps of intensities through the beam profile at the specular surface. Unfortunately, the profiles encountered are usually so erratic that the mere reporting of one test, let alone test-to-test correlation, is extremely cumbersome. Therefore a need exists to identify an "ideal-beam'equivalent" for the actual beam of each test.

The physical output of an IR-scanning camera is an analog (magnetic) tape. This memorandum will trace the techniques and software developed by BRL to take the analog information and arrive at contour plots, "equivalent beams", and three-dimensional prospective pictures.

II. DATA REDUCTION PROCEDURE

The steps in the data reduction sequence are shown in the flow diagram in Figure 1.

In step 1, the analog tape is digitized. The analog tape is formatted as follows: Each frame begins with a frame synch pulse; similarly each line scan (22 lines on the BRL IR Scanning Camera) begins with a line synch pulse. These synch pulses are superimposed on the continuous analog signal, with a frame synch pulse occuring every 0.008 seconds for the BRL scanner. Each line is then sampled at 42 equally spaced intervals in an apparent 22 x 42 matrix. However, timing problems result in the first line being entirely dropped (much like the retrace blanking is done on a television receiver). Further, a line synch pulse ringing problem necessitates zeroing out the first three samples on each line. The resulting scanner matrix is thus 21 x 42, with non-zero data in 21 x 39 samples.

The digitizing for BRL-processed-scanner data is accomplished in a mobile data acquisition system. The digitizing procedure results in a 9-track digital tape consisting of seven packed 16-bit words followed by 882 8-bit bytes. The 16-bit words contain such information as the run and frame number. The digitizing procedure also produces identification of the frame numbers corresponding to the start and stop of the laser beam.

Step 2 consists of taking the 9-track digitized data tape and transferring the information to a 7-track tape which can be accommodated on a UNIVAC 1108 computer. This is merely a system requirement and is accomplished by established system routines; no data reduction is involved.

In step 3 the program VLC performs the normalization discussed in Section I, and produces a line-printer contour plot of the normalized data. The time integrated raw data, plus certain terms are also dumped onto a binary tape. In step 4, the binary tape conveys the necessary data to the smoothing and fitting program, DRAPER.FIT. The results of DRAPER.FIT are available in synopsized form from the line printer. A comparison of the smoothed data to the DRAPER.FIT Gaussian is available in 3-dimensional prospective CALCOMP pictures from the program 3D-PLOT, shown as step 5. The VLC, DRAPER.FIT, and 3D-PLOT programs are discussed in the succeeding sections.

III. PROGRAM VLC

The program VLC performs five functions: (1) reads the digitized data tape and converts it to computer manageable integers; (2) determines the background noise and subtracts it from the raw data; (3) normalizes the raw data, as discussed in section I; (4) outputs line-printer contour

plots; and (5) produces a binary tape for use in step 4, Figure 1. The program consists of two routines: the main routine and IRTAPE, an assembly language tape interpreter.[1]

The inputs to VLC are shown in Table 1. The data tape must be called INPUT, the print file is unit 10, and the binary output tape is unit 12.

Referring to Table 1, the TEST Ident is any verbal phrase to appear as an output heading. FOV (field of view of the scanner) is the linear width (= height) of the scanner picture on the turning flat. Since the FOV is normally unchanged for several runs, the last inclusive run number for which a given FOV is to apply is input along with the FOV. A new FOV requires a new card input but not until after the data for the previous FOV's runs has been input.

BEAM ON and OFF FRAMES are obtained with the digitized tape and input as shown on Figure 1. The beam on/off card is also used to submit a start frame if, for example, the early frames are destroyed. For such cases, a $ in column 1 signifies that 3 integers follow.

The "number of time increments and values" card serves one of two functions; it either indicates the number of sequential time integrals to be made and their time intervals, or signals a calorimeter run. The latter requires 1, 0. on the time card; the time integral is then taken over the entire set of beam on/off frames. If the time card is 1, X where X does not equal 0., a component run is assumed. In either case, if only one time is given, no further cards are required for that run. On the other hand, if more than one time is given, the next card identifies the shot sequence; e.g. shield, component #1, component #2. (This information is only used for headings and does not affect the data reduction.)

A detailed key to the hard copy output of the VLC program is given in Appendix A.

IV. SMOOTHING AND FITTING THE MEASURED BEAM

A. SMOOTHING

As discussed in section I, the beams being diagnosed are often pathologically indescribable. The irregular, unsymmetrical shapes are dotted by spikes containing little power but having peak intensities many times higher than the local average. An example of such a beam is shown in figure 2A and 2B. From an effects/damage experimental viewpoint, however, these spikes - if real - are often irrelevant.

[1] *Mr. John Kinch, USABRL, private communication.*

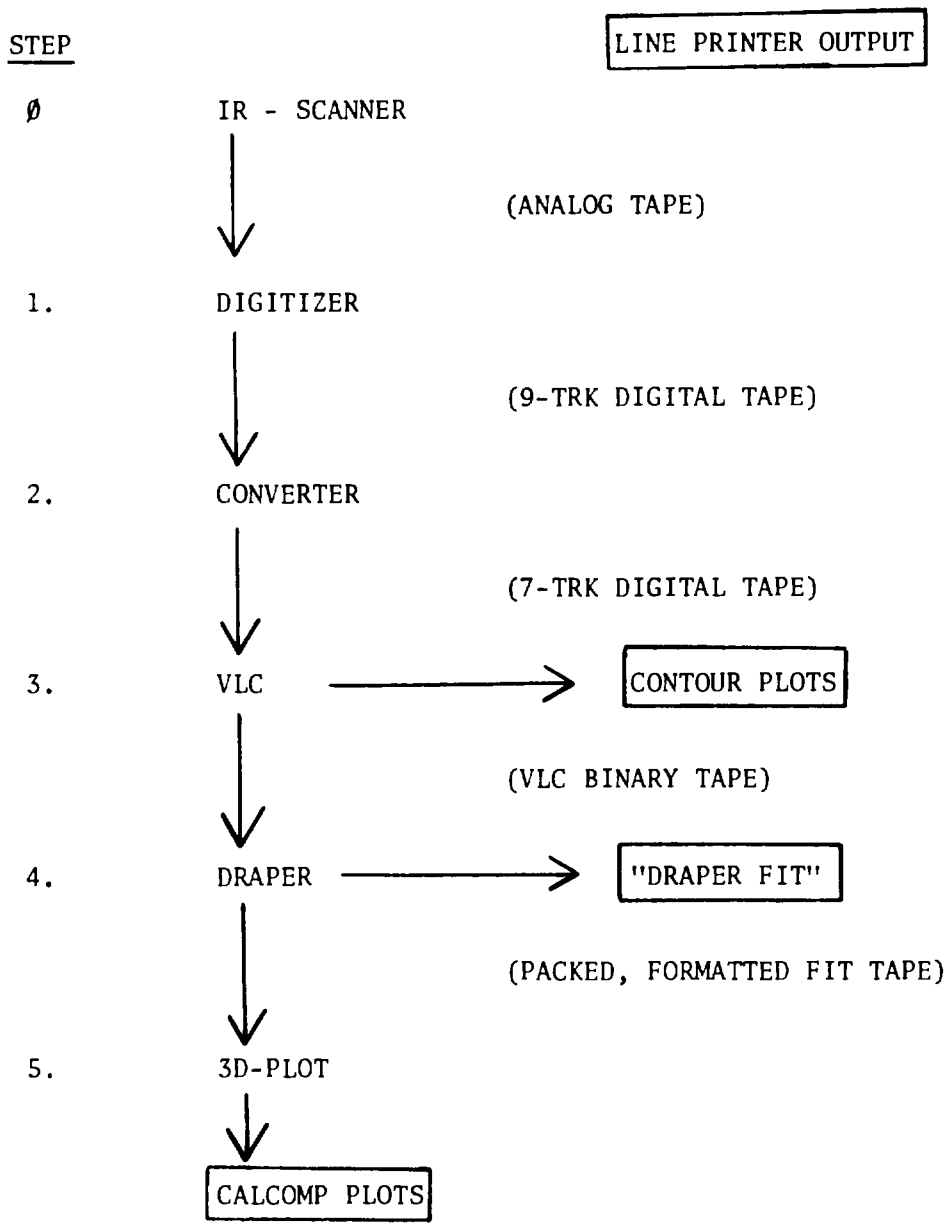

FIGURE 1. FLOW DIAGRAM

Table 1. VLC Inputs

Card No.

1. @XQT AMUCK * SCANNER.VLC
2. BRL SERIES 3A - TEST Ident.
3. 4.75, 2180 - FOV, last inclusive RUN NO.
4. 2175 - RUN NUMBER
5. 33, 296* - BEAM ON and OFF FRAMES
6. 75.3 - TOTAL POWER
7. 2, 0.5, 1.2 - Number of time incr & values
8. 2, 3 - Code corresponding to times

(USED ONLY IF .GT. 1 time is given above)

where 1 = CALORIMETER
2 = SHIELD
3 = COMPONENT #1
4 = COMPONENT #2

For a calorimeter test in which the beam intensity is to be averaged over the entire shot, the time card (#7) should be 1,0. since the number of time increments is only 1 and the code card (#8) is omitted.

9. 2176 - Same as #4
10. 29, 421 - Same as #5

.
.
.
.

29. 2180 - Same as #4
30. 37, 226 - Same as #5
31. 81.2 - Same as #6
32. 1, 0.5 - Same as #7
33. 5.25, 2191 - Same as #3

.
.

@EOF

UNIT	CONTAINS
INPUT	Data tape
10	Print file
12	Output binary

* Optional input for START/STOP card is $, 33, 296, 10 - BEAM ON and OFF, START FRAME

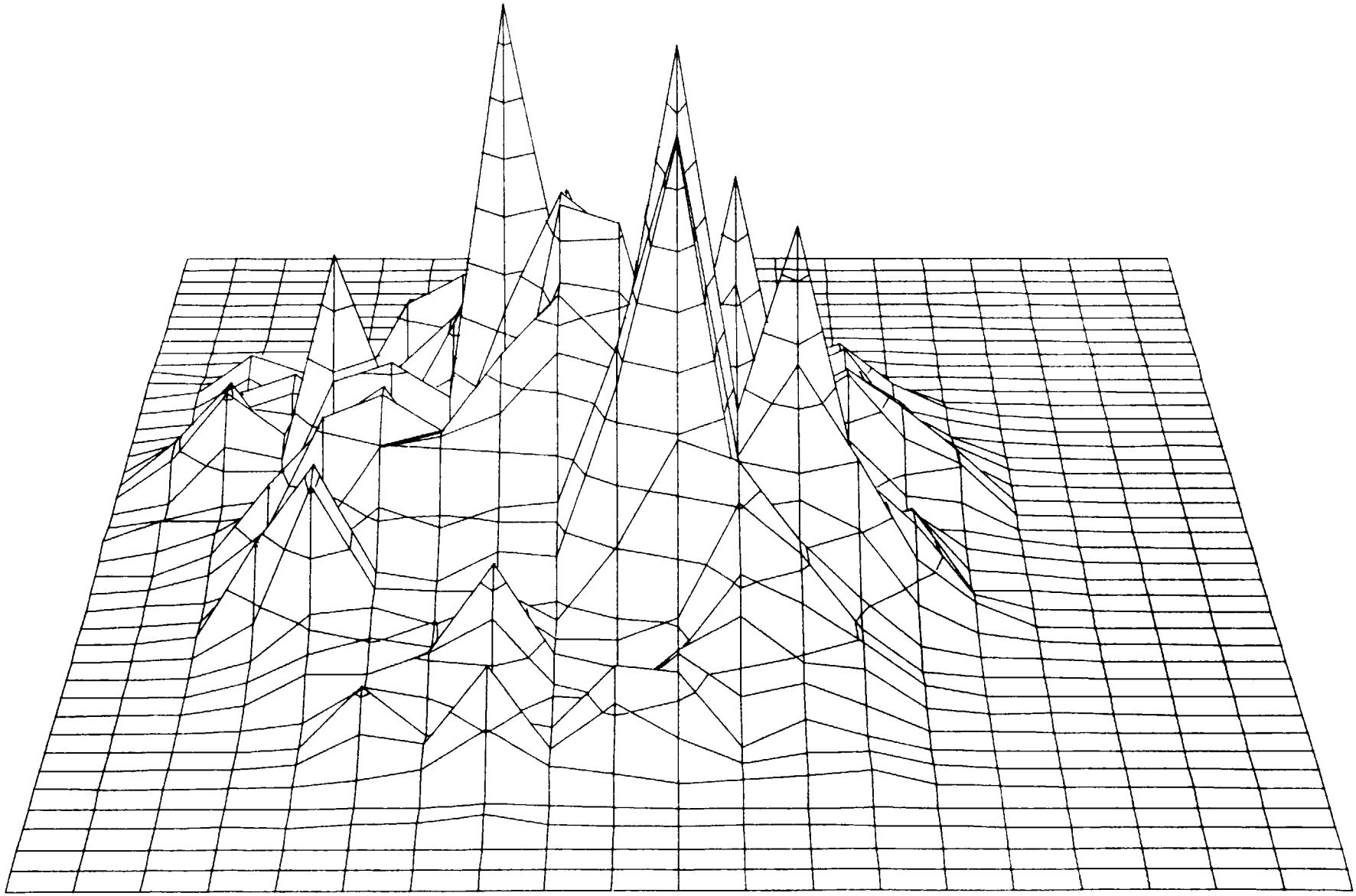

Figure 2A. Measured Beam Observed from the '21' Direction
Perspective of square field-of-view displayed 21 lines x 42 samples.

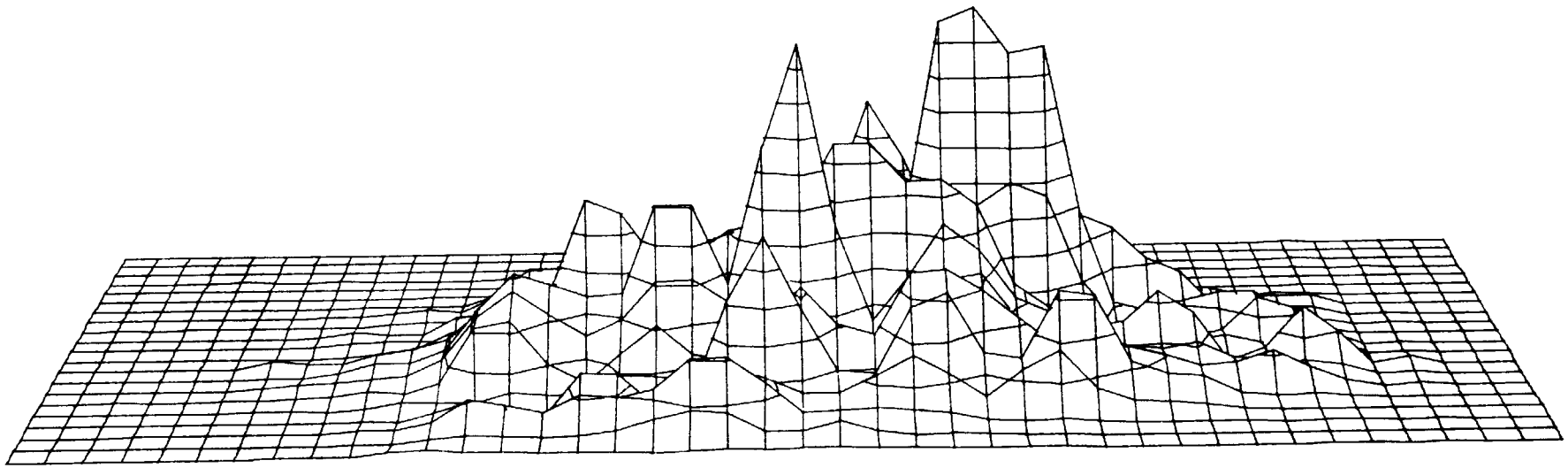

Figure 2B. Measured Beam Observed from the '42' Direction.
Perspective of square field-of-view displayed 21 lines x 42 samples.

(Note: Unpredictable errors, such as small irregularities on the mirror surface, could cause apparent spikes. Discussion of experimental error is, however, beyond the scope of this report.) Certain phenomena tend to spread out the beam power upon interaction with the target. Since the spikes contain little power, their effect, once spread, is minimal. It is therefore appropriate, as part of scanner data reduction, to show the effect of this spreading by applying a suitable smoothing to the raw data.

Often the most significant spreading phenomena is radial conduction. Therefore, to provide a lower bound on the smoothing, a simple radial conduction model was constructed. The model, presented in Appendix B, indicated that, for a typical experiment, resolution below 0.5 cm. at the target is probably superfluous. However, the model and attendant computer code can be run on a case by case basis.

The DRAPER.FIT program uses this resolution information. The analyst is queried for "X-cells over which to smooth" (recall - X is the line L direction; i.e., the 21 direction in the 21 x 42 output matrix.) The number of cells is found by determining a minimum resolution from the conduction model, and dividing that by the cell size as output by VLC. DRAPER.FIT then replaces each cell value by a weighted 2-dimensional average of local cells. The effect of averaging the beam of Figure 2 over one and two cells is shown in Figures 3 and 4 respectively.

B. FITTING

As seen from the above figures, the resulting beam is still not conveniently described. Test-to-test comparison of results is impossible because of the inability to quantitatively account for the important beam parameters. What is needed is an equivalent beam of a standard form to be equated to each measured actual beam. For operational reasons, a Gaussian is a preferrable standard form. The task then reduces to defining a technique for fitting an equivalent Gaussian to the smoothed beam profile data; i.e., finding the appropriate parameters for the form:

$$I(x,y) = I_o * \exp(-(x-x_o)^2/2R_x^2) * \exp(-(Y-Y_o)^2/2Ry^2) + B \qquad (1)$$

The crux of the problem lies in determining what is meant by "equivalent". For instance, a CHI-square minimization[2] program was used to fit equation 1 to some actual data. It was found that the area away

[2] *J.T. Klopcic, "FNFIT: An Easy-To-Use, Arbitrary Function-To-Data Fitting Routine (A User's Manual)," U.S. Army Ballistic Research Laboratory, BRL MR 2402 (1974).* (AD #A000655)

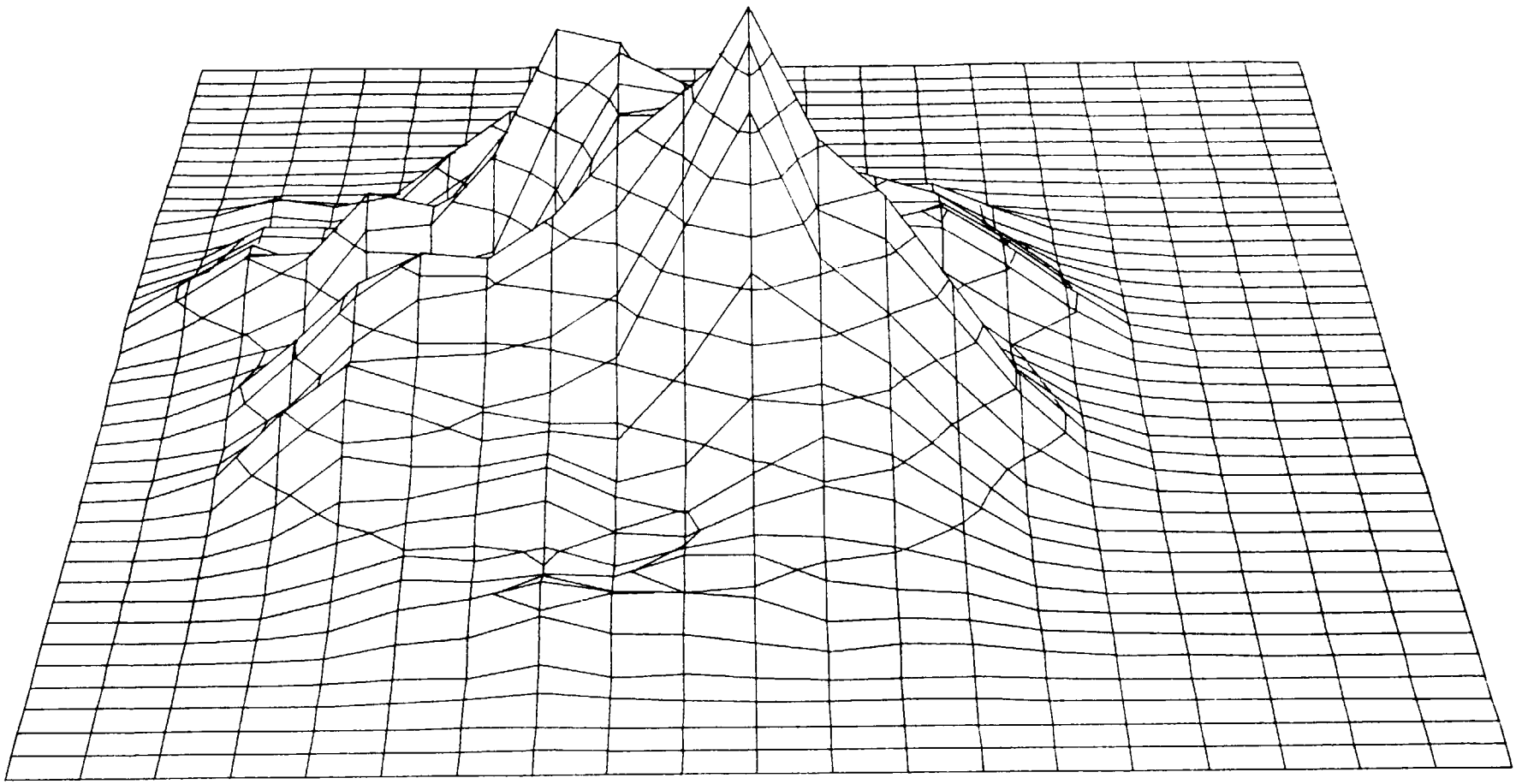

Figure 3A. Results of Averaging Over One Cell for Figure 2A
Perspective of square field-of-view displayed 21 lines x 42 samples.

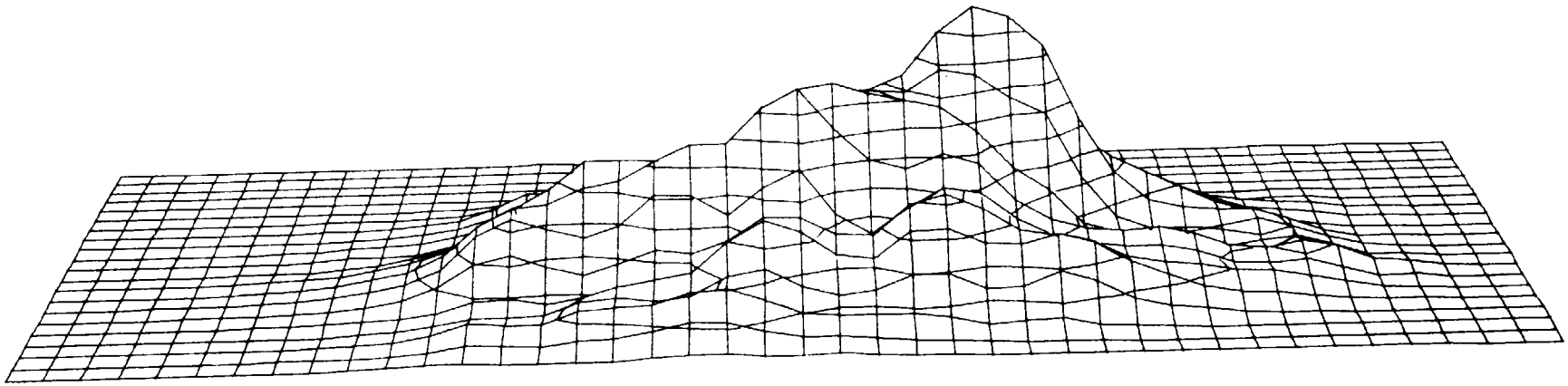

Figure 3B. Results of Averaging Over One Cell for Figure 2B
Perspective of square field-of-view displayed 21 lines x 42 samples.

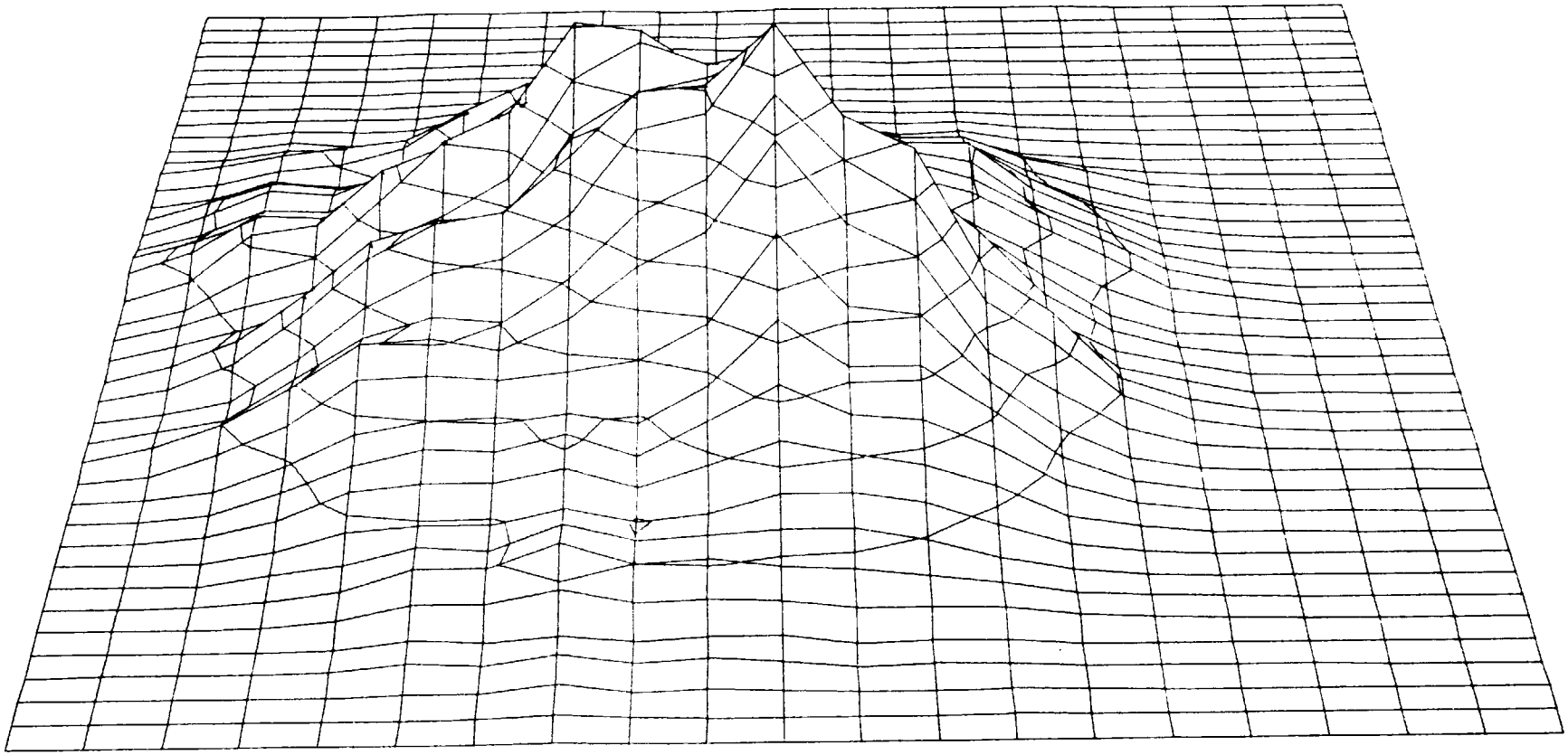

Figure 4A. Results of Averaging Over Two Cells for Figure 2A
Perspective of square field-of-view displayed 21 lines x 42 samples.

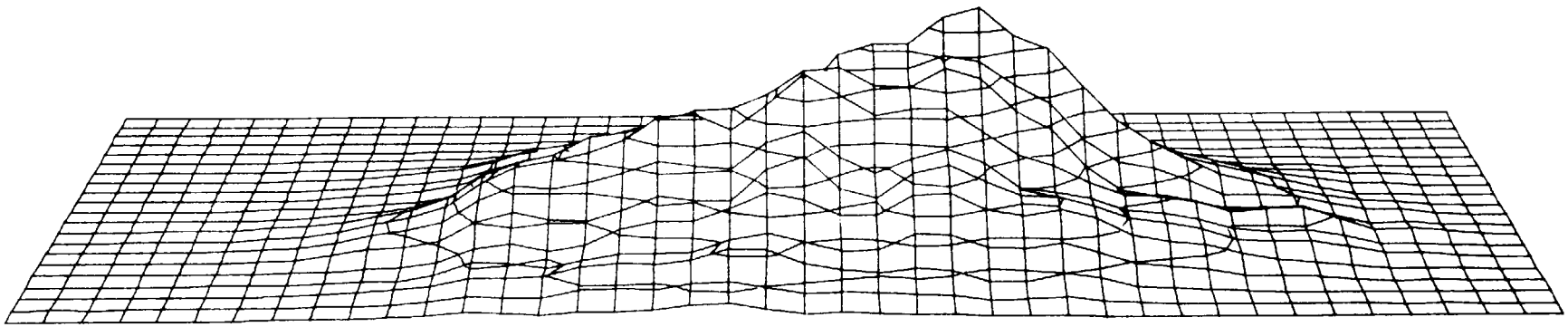

Figure 4B. Results of Averaging Over Two Cells for Figure 2B
Perspective of square field-of-view displayed 21 lines x 42 samples.

from the peak dominated the fit, resulting in values for I_o which were clearly too small to be indicative of the actual beam. The I_o was improved by weighting each data point by $Z(I)^{\alpha}$, where $Z(I)$ is the (intensity) value at the point, and α is a positive number. As expected, the value of I_o more closely approached the height of the dominant peaks as larger values for α (e.g., 1.0, 1.5, 2.0, 3.0) were investigated. Unfortunately, the arbitrary choice of values for α was unacceptable, and other definitions of equivalent were sought.

Another possible approach to defining an equivalent Gaussian is to determine various characteristics of the actual beam, and choose a Gaussian having the same values for those characteristics. Examples of such characteristics are the mean and standard deviation. If as many (independent) characteristics are chosen as there are parameters in the Gaussian (six in equation 1), then the Gaussian is uniquely determined.

A possible set of six characteristics is shown in Table 2.

Table 2. Beam Characteristics (Power)

1. $\int_{A'} I(x,y,t)\cdot dA\cdot dt = C \cdot \int_{A'} dA\cdot dt$, A' outside $2\sigma_x$, $2\sigma_y$

2, 3. $\mu_x = \int x\cdot I(x,y,t)dA\cdot dt/E$; $\mu_y = \int y\cdot I(x,y,t)\cdot dA\cdot dt$

4, 5. $\sigma_x^2 = \int (x-\mu_x)^2 \cdot I(x,y,t)\cdot dA\cdot dt \;/\; E$

$\sigma_y^2 = \int (y-\mu_y)^2 \cdot I(x,y,t)\cdot dA\cdot dt \;/\; E$

6. $E = \int I\,(x,y,t)\cdot dA\cdot dt$

Characteristic 1 is a definition of background, and establishes a baseline level (C). Characteristics 2 and 3 define the mean, and 4 and 5 define the variance. E is recognized as the total energy delivered. Therefore, characteristic 6 assures that the total power of the equivalent Gaussian is equal to the (time averaged) total power of the beam.

The integrals involved above can be done in closed form for the Gaussian of equation 1, yielding the expressions for the six characteristics shown in Table 3.

Table 3. Gaussian Values for Beam Characteristics (Power)

1. $B \simeq C$

2, 3. X_o, Y_o = means (μ_x, μ_y)

4, 5. R_x^2, R_y^2 = variances (σ_x^2, σ_y^2)

6. $2 \cdot \pi \cdot R_x \cdot R_y \cdot I_o \cdot t = E$

The POWER option of the DRAPER.FIT program calculates the equivalent Gaussian via these six criteria. The characteristics C, μ_x, μ_y, σ_x, σ_y, and E are evaluated from the digitized frames by performing the needed spatial and temporal integrations numerically. The relations shown in Table 3 are then used to compute the equivalent Gaussian parameters X_o, Y_o, R_x, R_y, I_o and B.

The results of fitting the beams of Figures 2, 3 and 4 via this technique are shown in Figures 5, 6, and 7. DRAPER.FIT also gives information printed along the left margin of the picture (see Appendix C). The order and meaning of the information is given in Appendix C. Finally, DRAPER.FIT also gives a CHI-SQ for each fit, where CHI-SQ is defined as

$$\text{CHI-SQ} = N * \sum_{I=1}^{NDATA} (Z_I - I(X_I, Y_I))^2 / I^2(X_I, Y_I) \qquad (2)$$

where $N = 1 / (NDATA - 7)$

For the fits in Figures 5, 6 and 7, the CHI-SQ values were 0.644, 0.471 and 0.404 respectively. No absolute interpretation for CHI-SQ is put forth here in terms of statistical confidence levels; rather, CHI-SQ is used as a relative measurement. (Recall that the CHI-SQ minimization approach was unsatisfactory.) As such, the CHI-SQ indicates the improvement in fit with smoothing, as seen in Figures 5, 6 and 7.

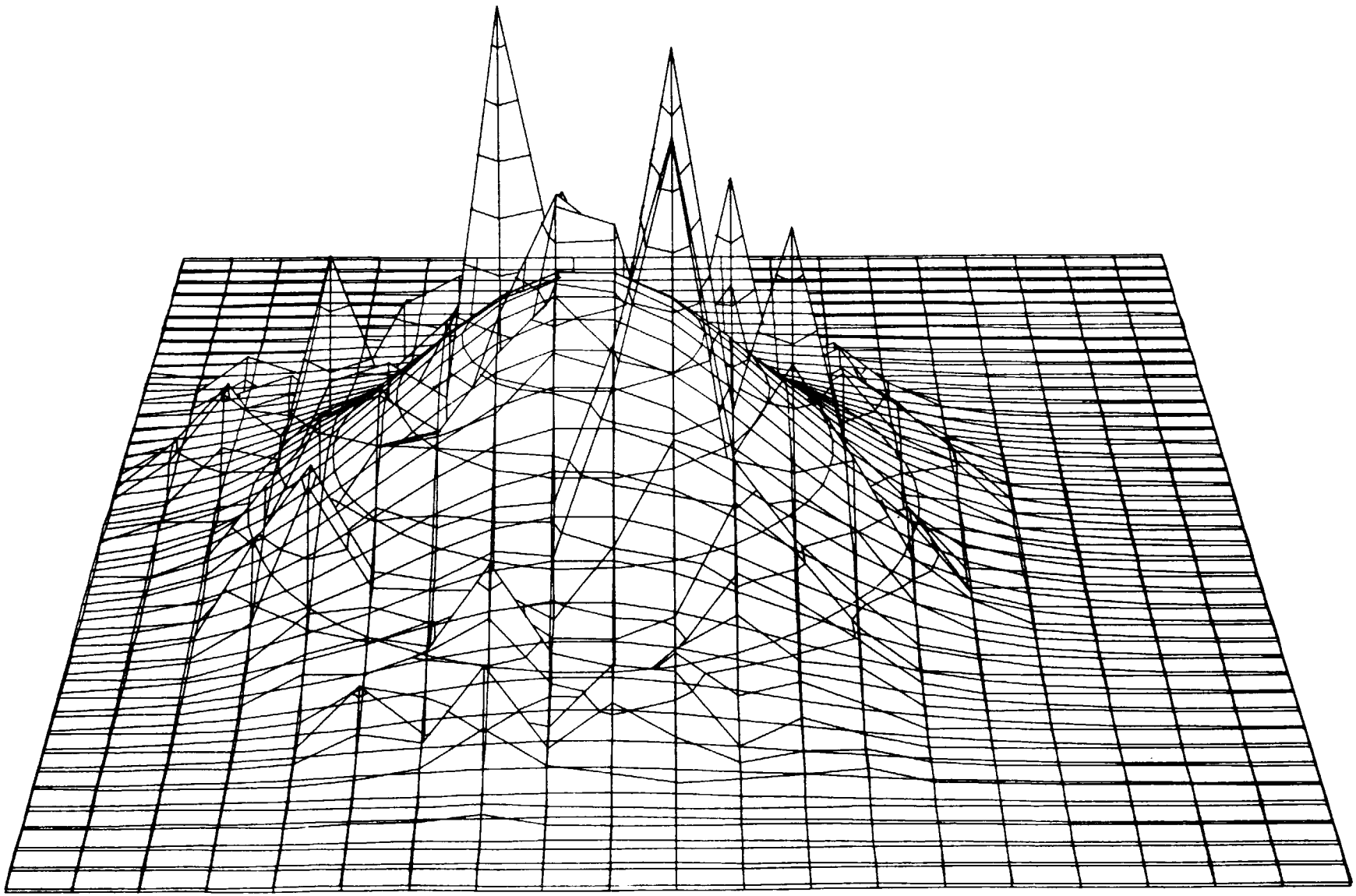

Figure 5A. DRAPER.FIT (Power Option) for Figure 2A
Perspective of square field-of-view displayed 21 lines x 42 samples.

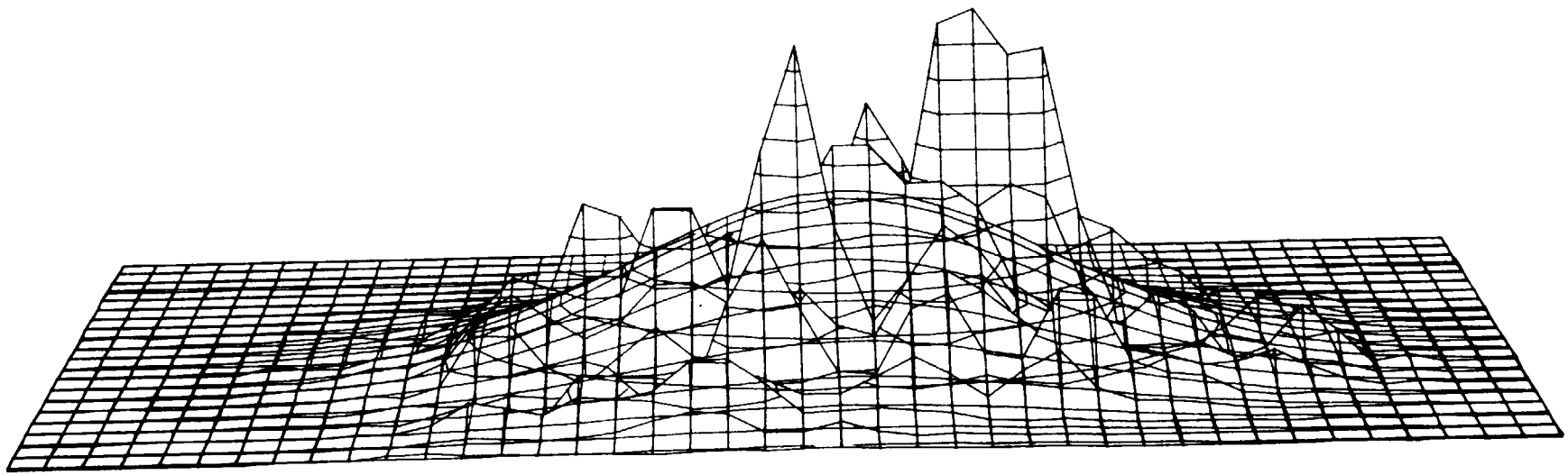

Figure 5B. DRAPER.FIT (Power Option) for Figure 2B
Perspective of square field-of-view displayed 21 lines x 42 samples.

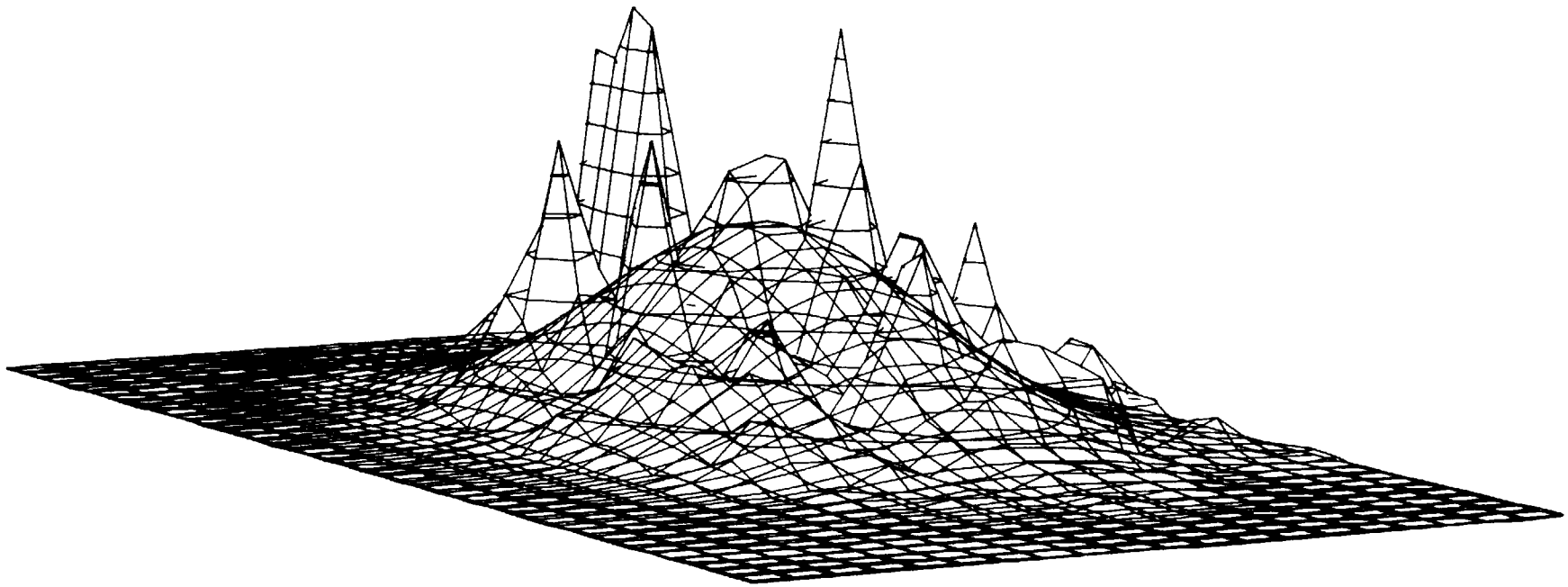

Figure 5C. DRAPER.FIT (Power Option) for Figure 2A Oriented Clockwise 45 Degrees
Perspective of square field-of-view displayed 21 lines x 42 samples.

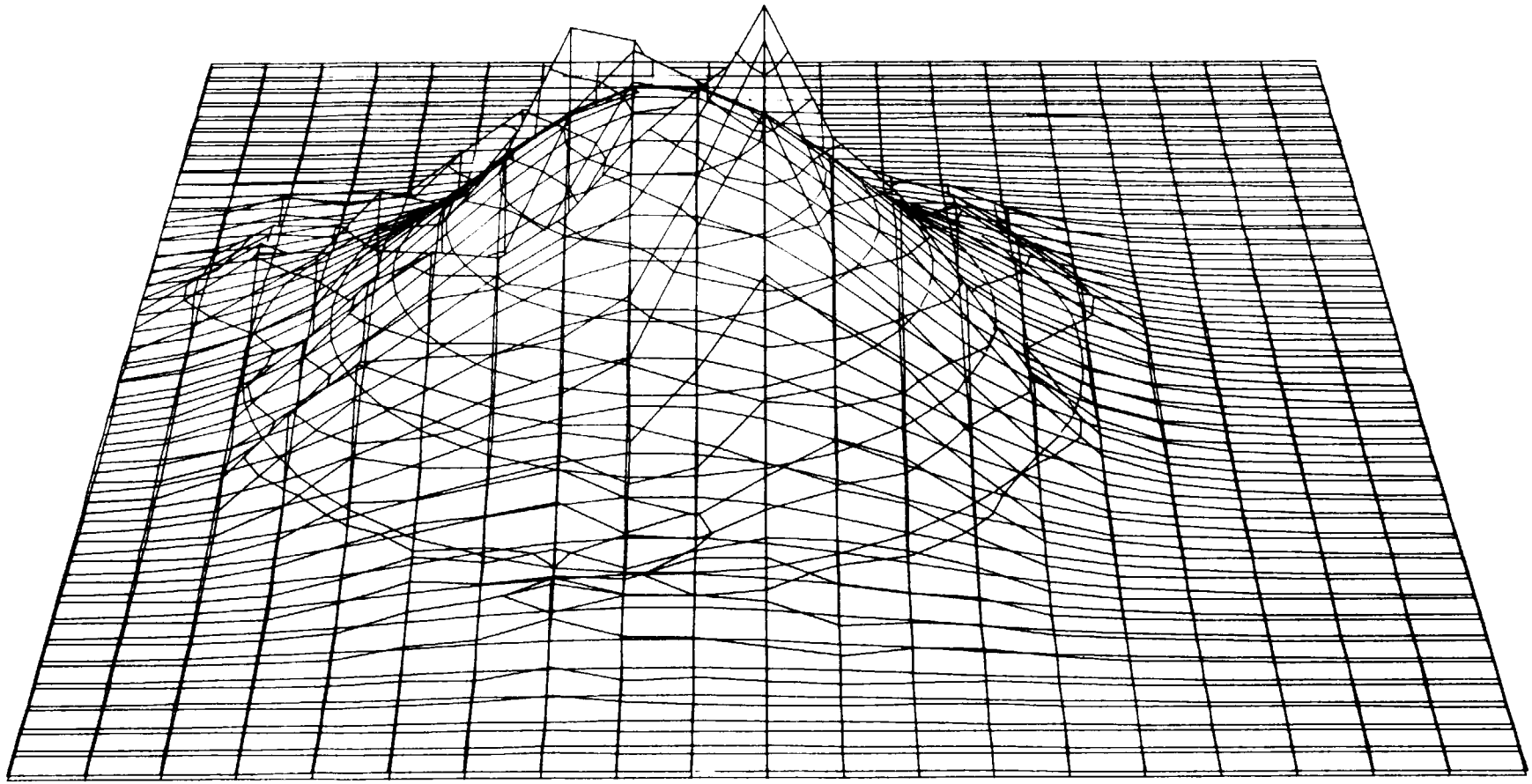

Figure 6A. DRAPER.FIT (Power Option) for Figure 3A
Perspective of square field-of-view displayed 21 lines x 42 samples.

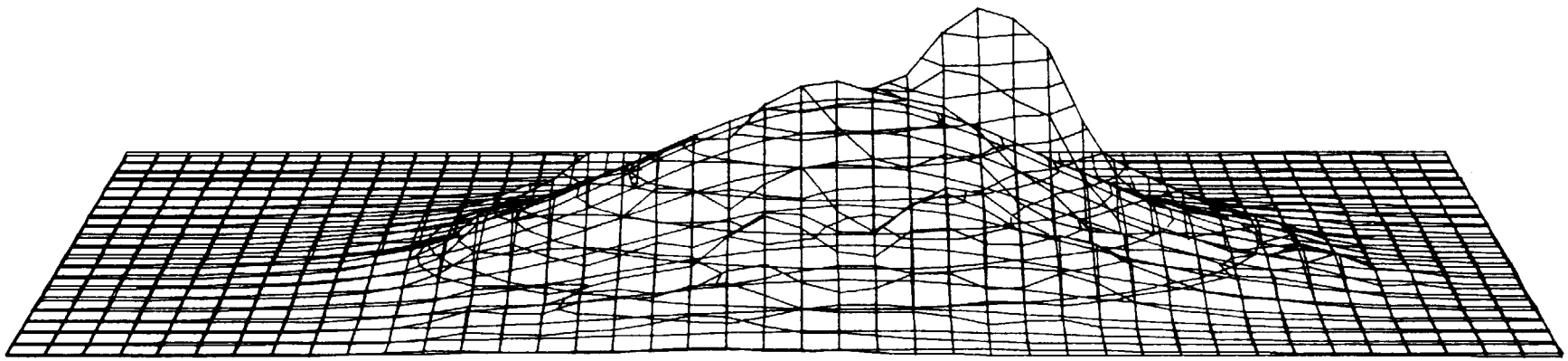

Figure 6B. DRAPER.FIT (Power Option) for Figure 3B
Perspective of square field-of-view displayed 21 lines x 42 samples.

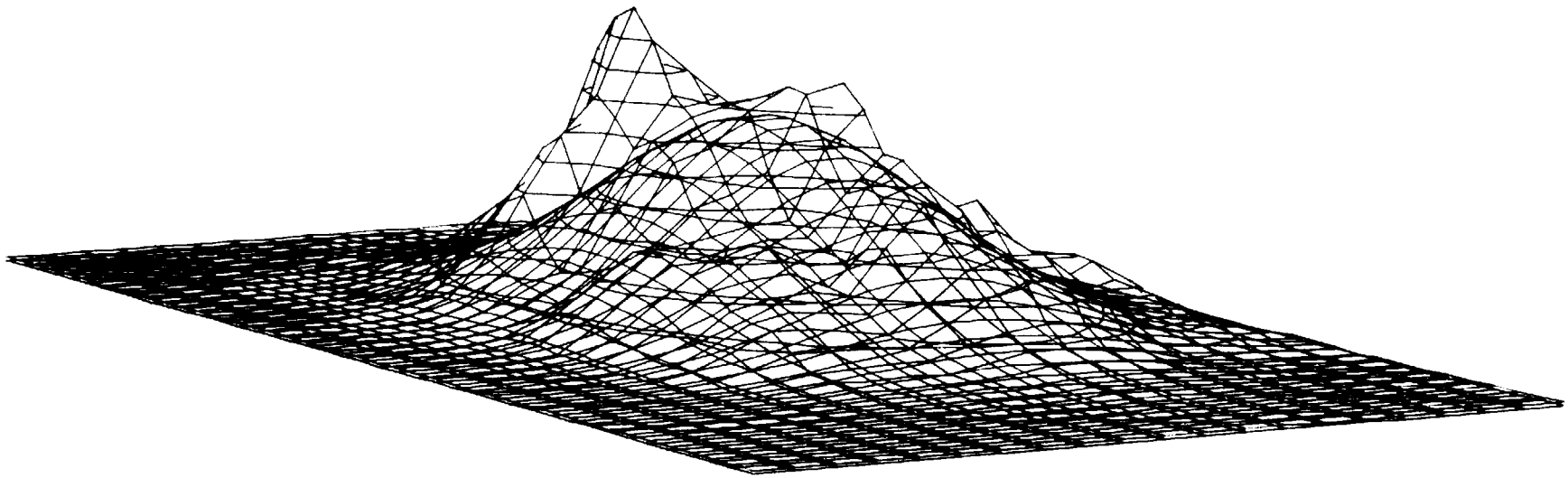

Figure 6C. DRAPER.FIT (Power Option) for Figure 3A Oriented Clockwise 45 Degrees
Perspective of square field-of-view displayed 21 lines x 42 samples.

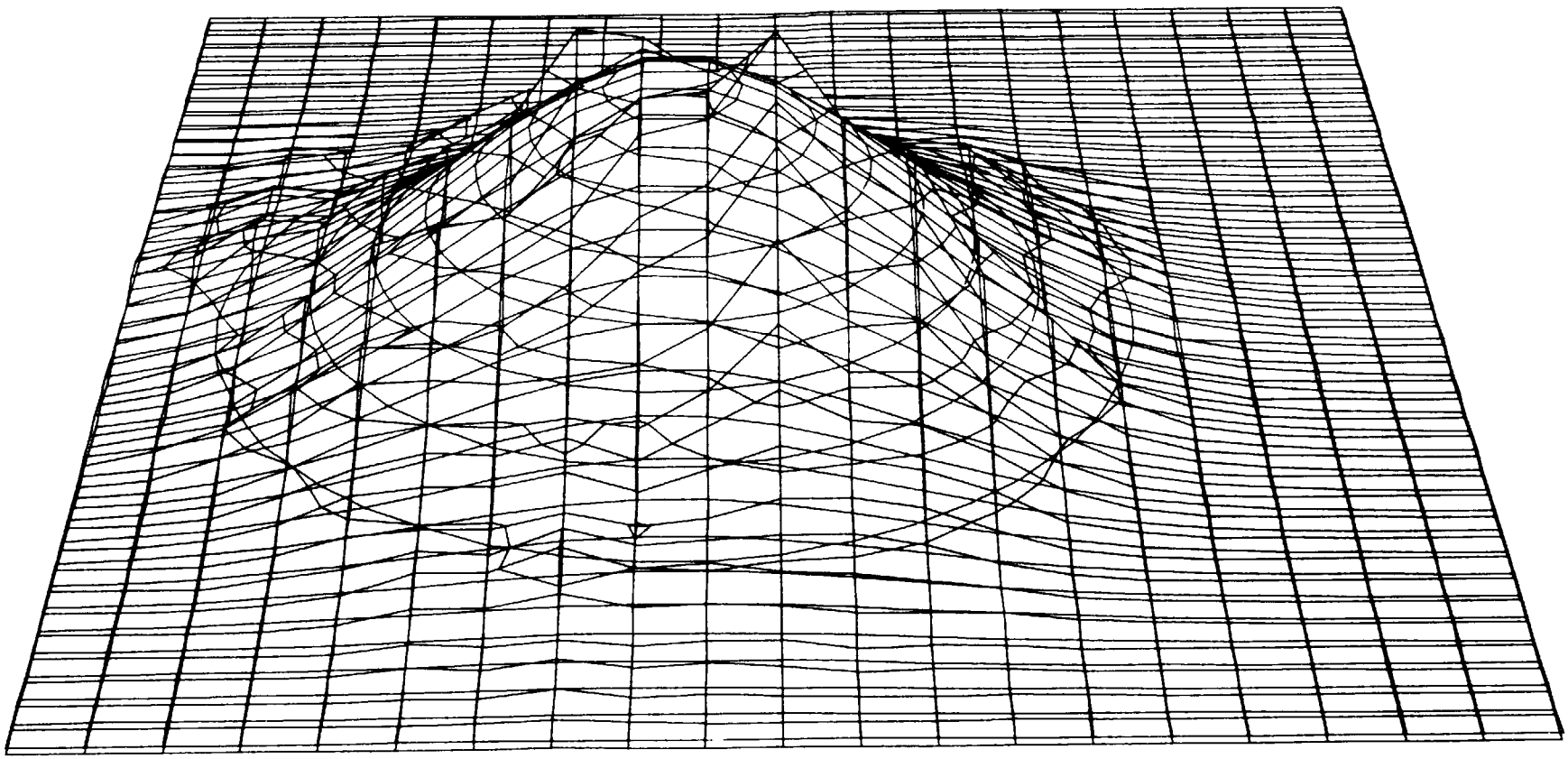

Figure 7A. DRAPER.FIT (Power Option) for Figure 4A
Perspective of square field-of-view displayed 21 lines x 42 samples.

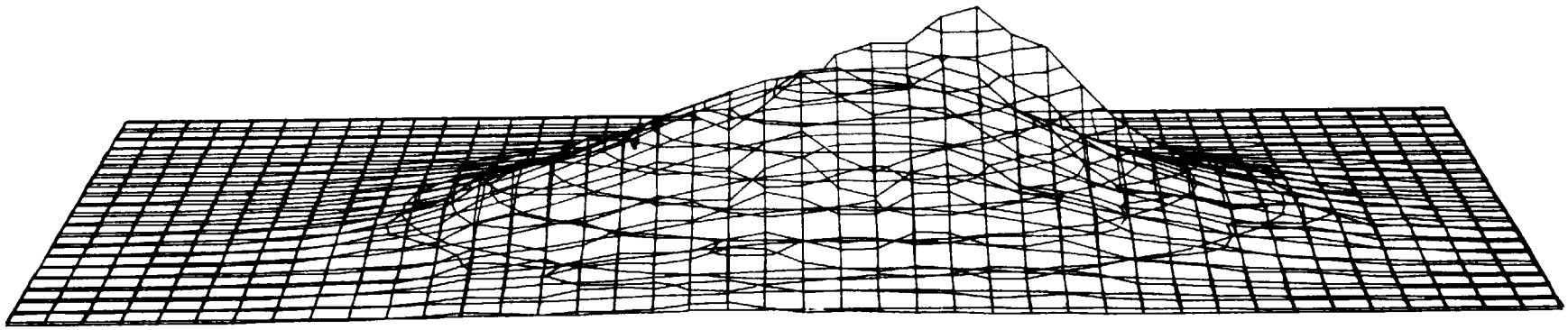

Figure 7B. DRAPER.FIT (Power Option) for Figure 4B
Perspective of square field-of-view displayed 21 lines x 42 samples.

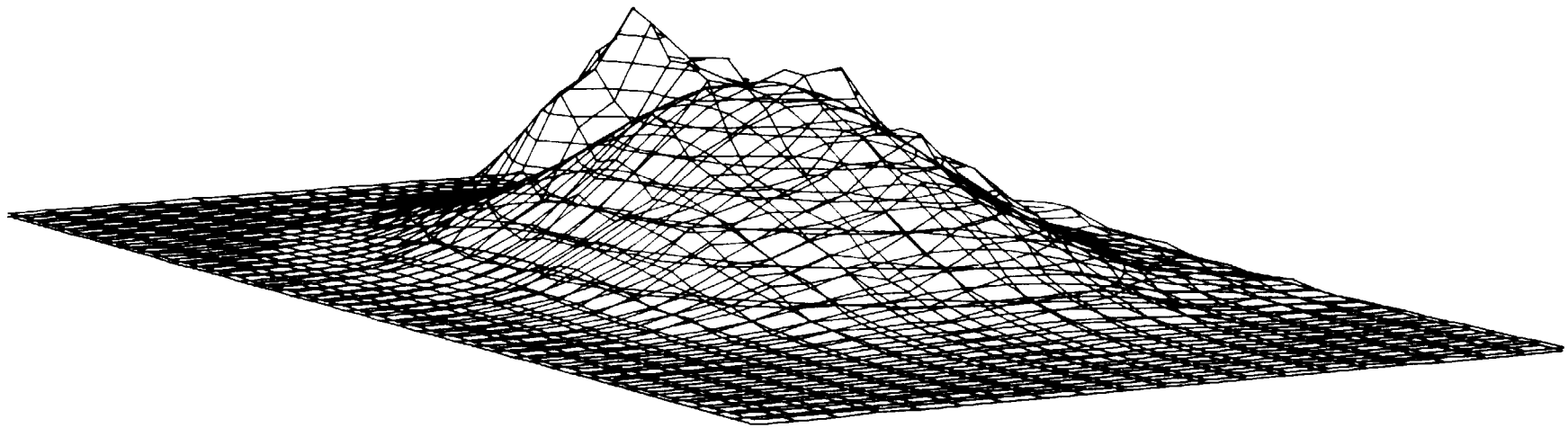

Figure 7C. DRAPER.FIT (Power Option) for Figure 4A Oriented Clockwise 45 Degrees
Perspective of square field-of-view displayed 21 lines x 42 samples.

The choice of characteristics upon which to base the fit is, as implied above, somewhat arbitrary. For the reporting of damage and effects data, the "DRAPER characteristics", a set slightly different from that in Table 2, is preferred.

In a report on parameter sensitivity analysis considerations by the Charles Stark Draper Laboratories,[3] a discussion of beam characterization was presented. In particular, it was noted that the term I(x,y,t) serves as a distribution function for the calculation of $\bar{x}$ and $\bar{s}$ (μ and σ). One is then led to define an average intensity, $\bar{I}$, analogously.

$$\bar{I} = \int I(x,y,t) \cdot I(x,y,t) \cdot dA \cdot dt \; / \; E \qquad (3)$$

The Draper report went on to discuss the behaviour of this $\bar{I}$ for a set of idealized beams, showing that the damaging potential of the beams was appropriately ranked by $\bar{I}$.

The Draper observations were embraced by the equivalent Gaussian portion of the scanner program. $\bar{I}$ constitutes a characteristic of the beam in the sense of those in Table 2, with the added benefit that $\bar{I}$ is a reflection of damage potential. Furthermore, substituting $\bar{I}$ for E (characteristic 6 in Table 2) results in a complete and mutually independent set, as listed in Table 4.

Table 4. Beam Characteristics (Draper)

1. $\int_{A'} I(x,y,t) \cdot dA \cdot dt = C \cdot \int_{A'} dA \cdot dt$, A' outside $2\sigma_x$, $2\sigma_y$

2,3. $\mu_x = \int x \cdot I(x,y,t) dA \cdot dt / E$; $\mu_y = \int y \cdot I(x,y,t) \cdot dA \cdot dt$

4,5. $\sigma_x^2 = \int (x-\mu_x)^2 \cdot I(x,y,t) \cdot dA \cdot dt \; / \; E$

$\sigma_y^2 = \int (y-\mu_y)^2 \cdot I(x,y,t) \cdot dA \cdot dt \; / \; E$

6. $\bar{I} = \int [I(x,y,t)]^2 \cdot dA \cdot dt \; / \; E$

[3] *Olsson, Ouellette, et al., "Parameter Sensitivity Analysis," the Charles Stark Draper Laboratory, Inc., SER# 009-05-346 (June 1975).*

As in the POWER normalized case, the expression for $\bar{I}$ for the Gaussian of equation 1 is

$$\bar{I} = (\pi \cdot R_x \cdot R_y \cdot I_o^2 \cdot t) / E = I_o / 2 \qquad (4)$$

The counterpart to Table 3 is presented as Table 5.

Table 5. Gaussian Values for Beam Characteristics (DRAPER)

1. $B \approx C$

2,3. X_o, Y_o = means (μ_x, μ_y)

4,5. R_x^2, R_y^2 = variances (σ_x^2, σ_y^2)

6. $I_o = 2 \cdot \bar{I}$

The beams of Figures 2-4 are presented with their DRAPER.FIT in Figures 8-10. As expected, the DRAPER.FIT results more closely fit the peaks. The overall fits, as determined by the CHI-SQ criterion, are better, especially for the unsmoothed beam. CHI-SQ values for Figures 8, 9 and 10 are 0.558, 0.449, and 0.394 respectively.

The DRAPER.FIT computer program is an interactive routine which solicits desired inputs in free field format. The input routine directly reads the output tape from VLC program. Outputs of the DRAPER.FIT program include line printer copy (alternate print file 7 optional), and a tape compatible with the 3D-PLOT routine.

V. PROGRAM 3D-PLOT

The 3D-PLOT routine does no data processing. However, as can be seen by comparing Figures 2-10 with Figure A-1 in Appendix A, the interpretation of scanner data is markedly assisted by graphical displays.

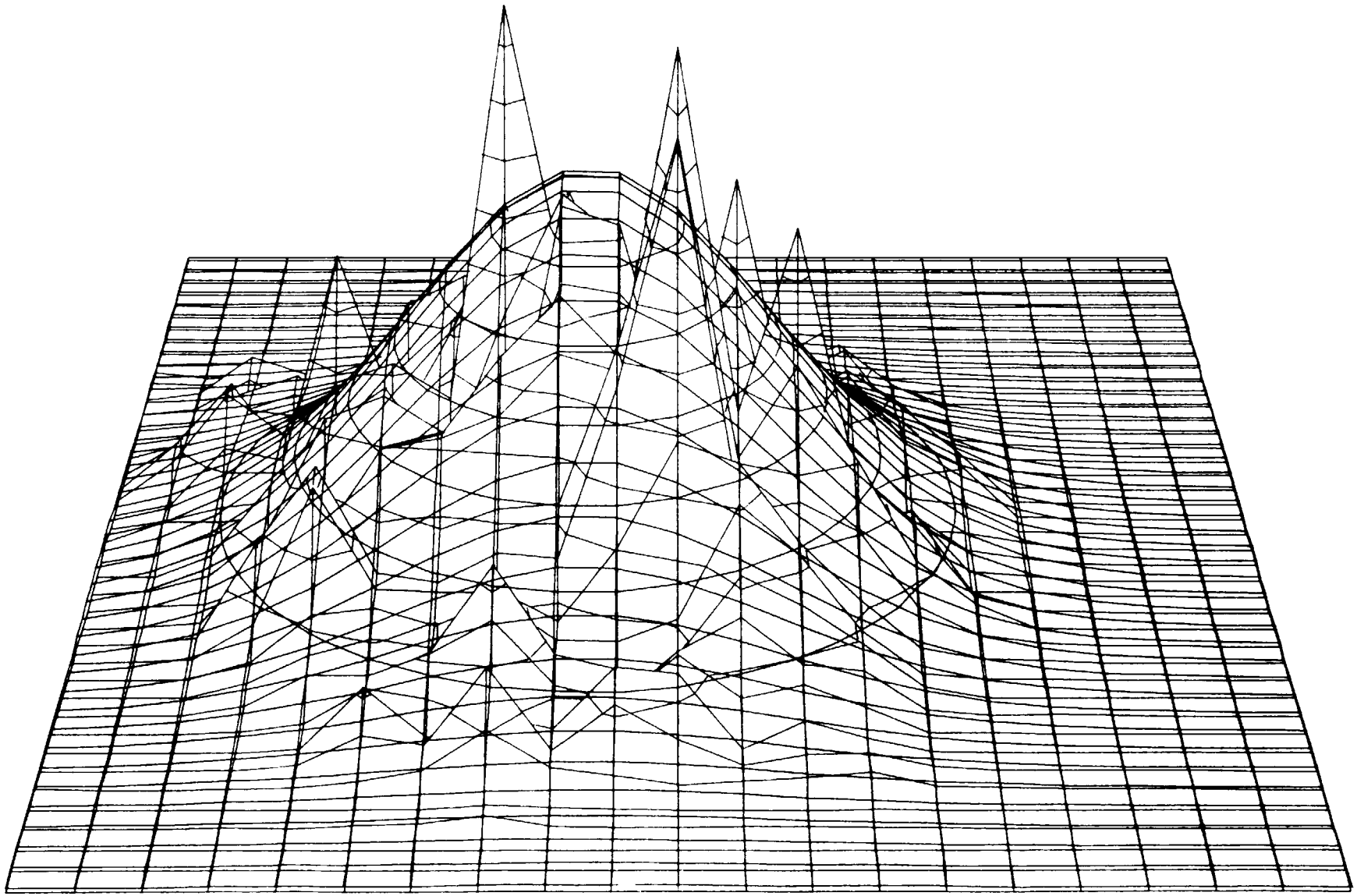

Figure 8A. DRAPER.FIT (Gaussian) for Figure 2A
Perspective of square field-of-view displayed 21 lines x 42 samples.

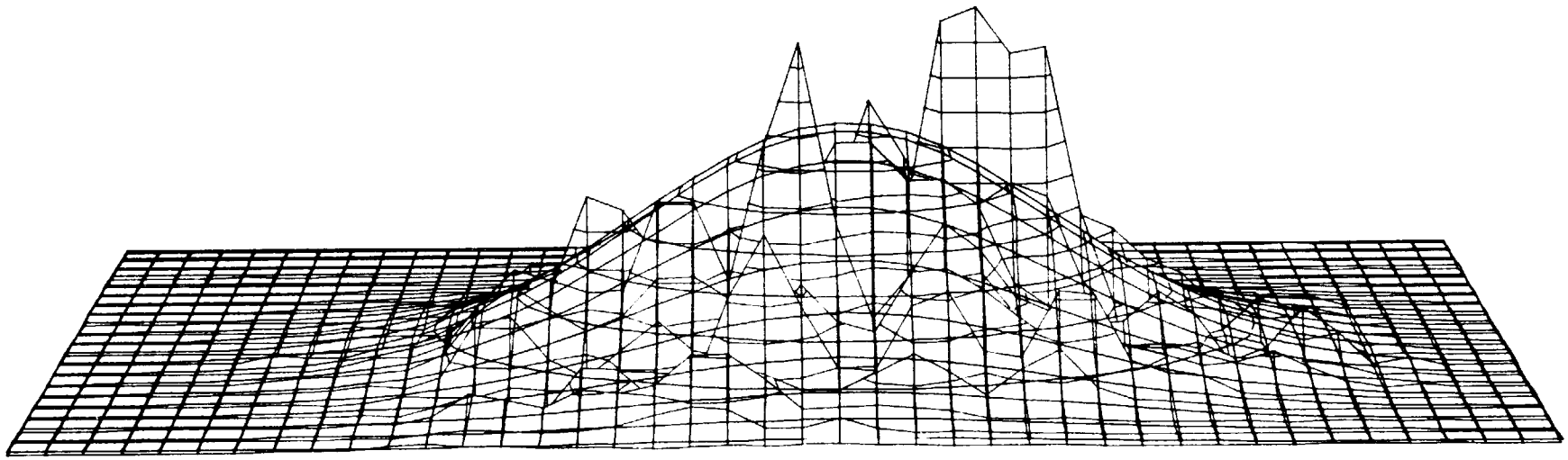

Figure 8B. DRAPER.FIT (Gaussian) for Figure 2B
Perspective of square field-of-view displayed 21 lines x 42 samples.

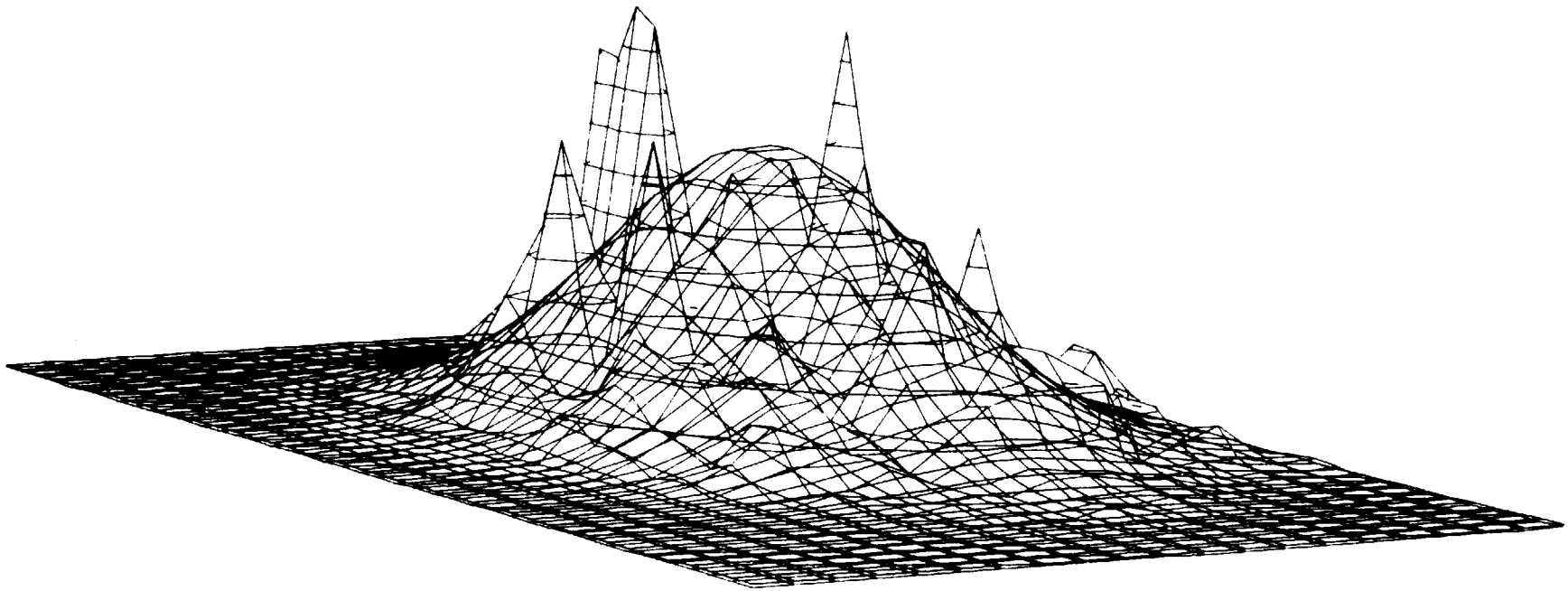

Figure 8C. DRAPER.FIT (Gaussian) for Figure 2A Oriented Clockwide 45 Degrees
Perspective of square field-of-view displayed 21 lines x 42 samples.

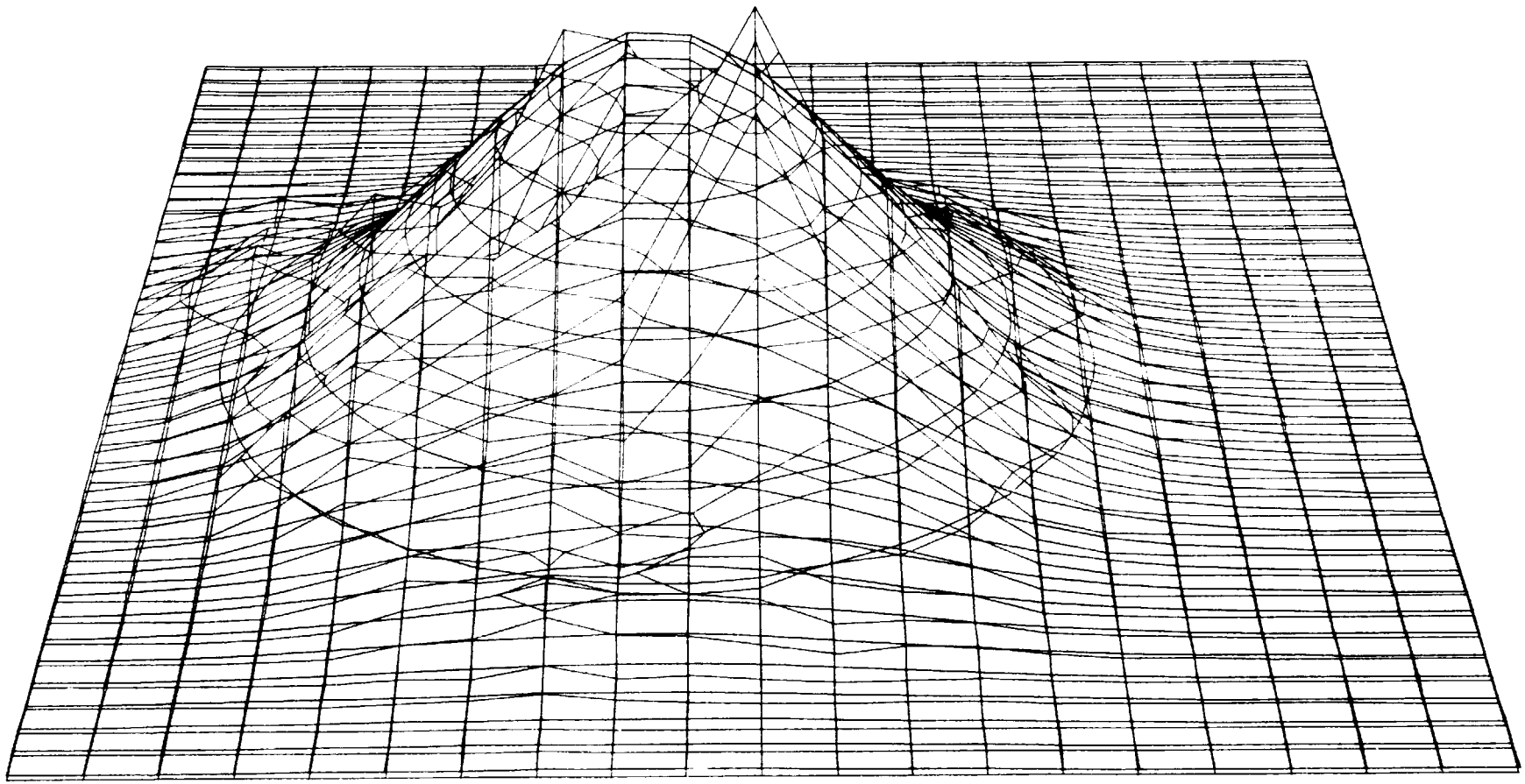

Figure 9A. DRAPER.FIT (Gaussian) for Figure 3A
Perspective of square field-of-view displayed 21 lines x 42 samples.

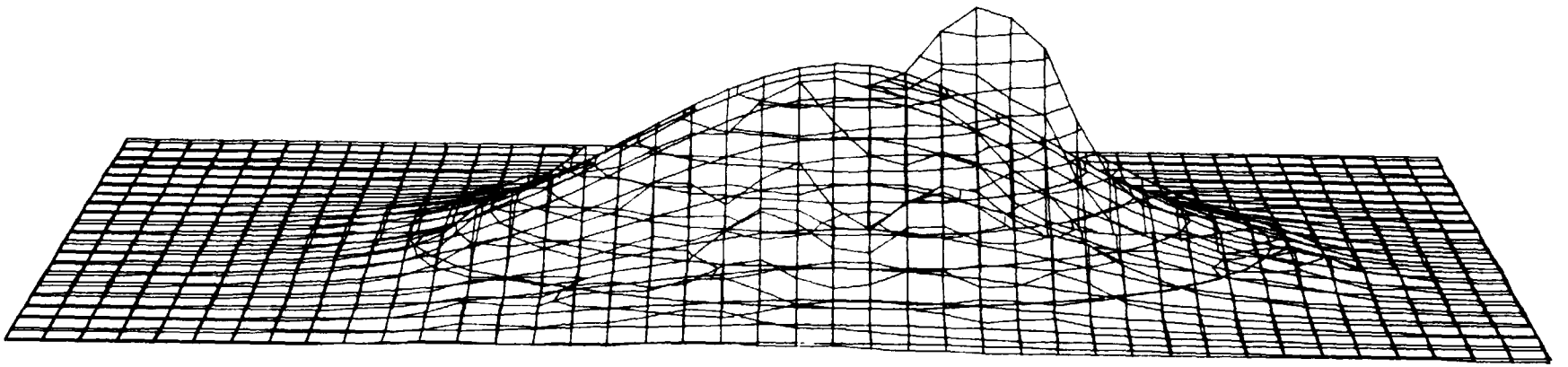

Figure 9B. DRAPER.FIT (Gaussian) for Figure 3B
Perspective of square field-of-view displayed 21 lines x 42 samples.

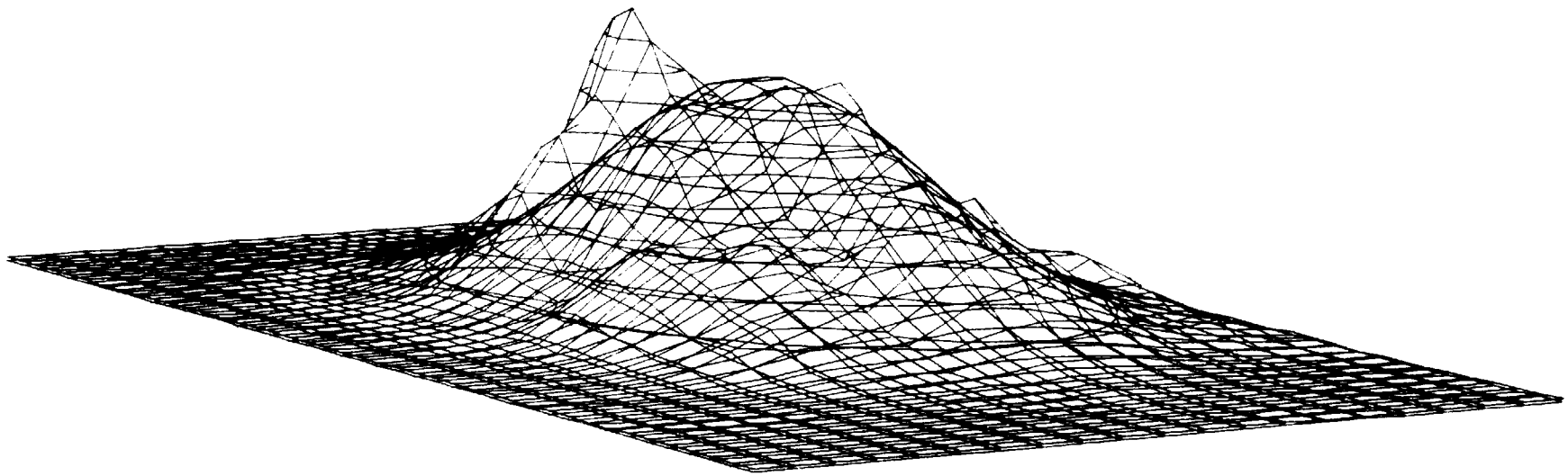

Figure 9C. DRAPER.FIT (Gaussian) for Figure 3A Oriented Clockwise 45 Degrees
Perspective of square field-of-view displayed 21 lines x 42 samples.

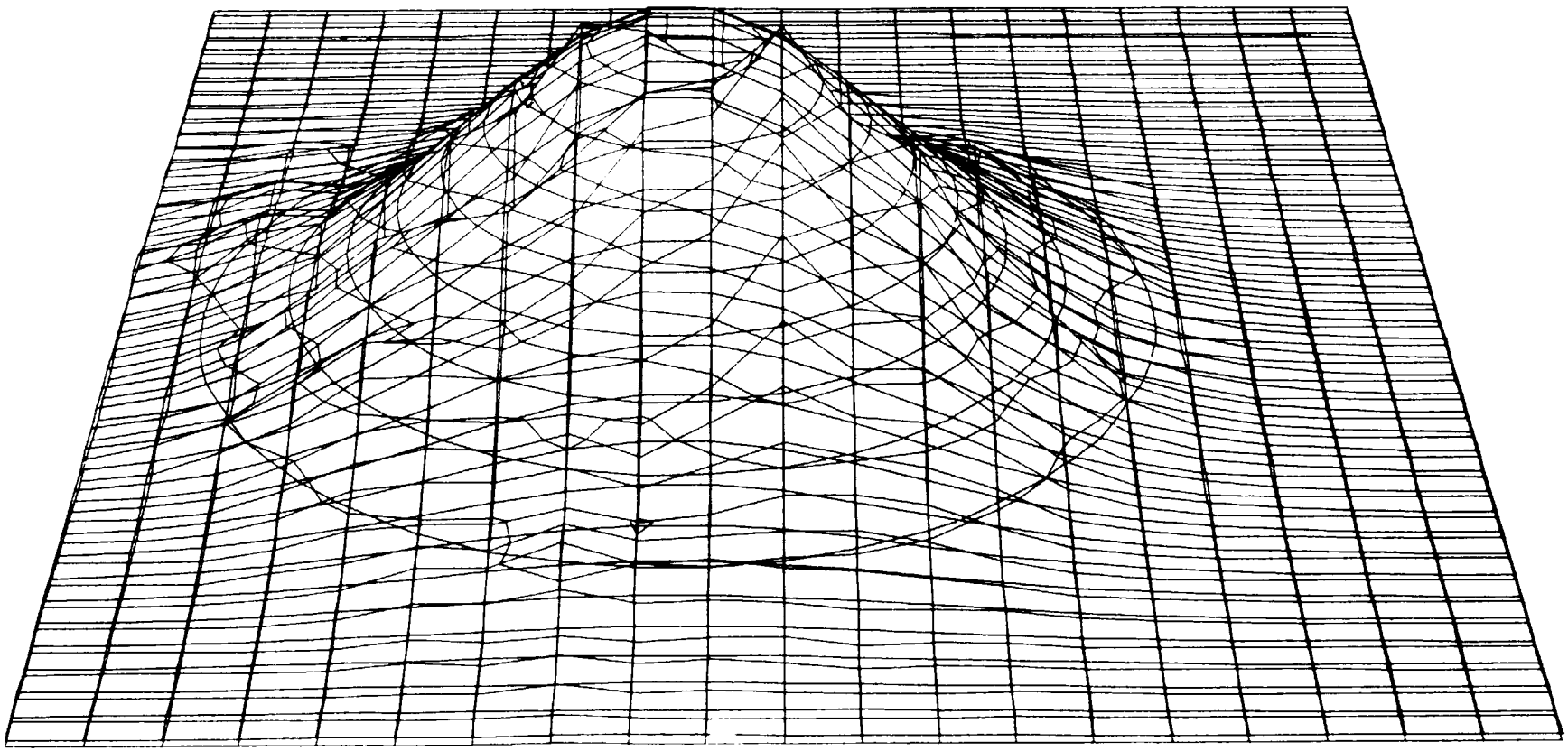

Figure 10A. DRAPER.FIT (Gaussian) for Figure 4A
Perspective of square field-of-view displayed 21 lines x 42 samples.

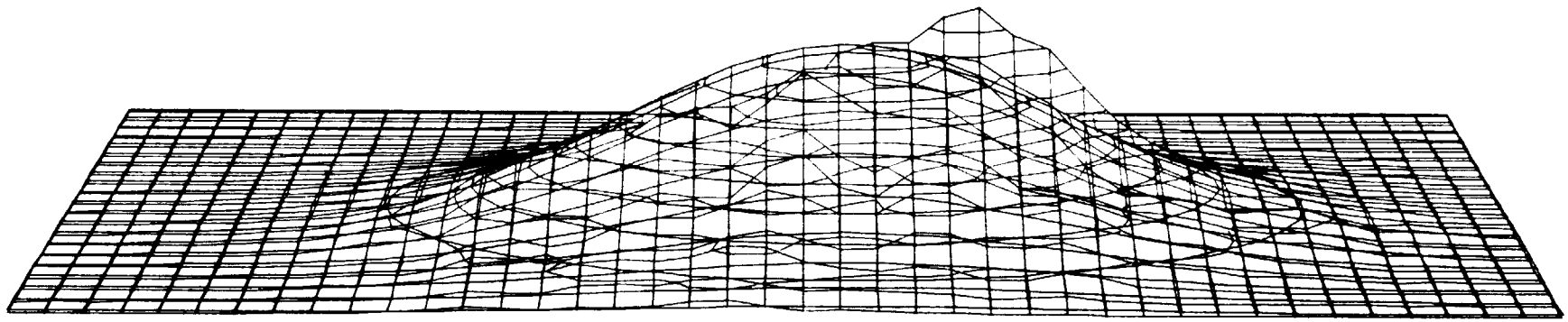

Figure 10B. DRAPER.FIT (Gaussian) for Figure 4B
Perspective of square field-of-view displayed 21 lines x 42 samples.

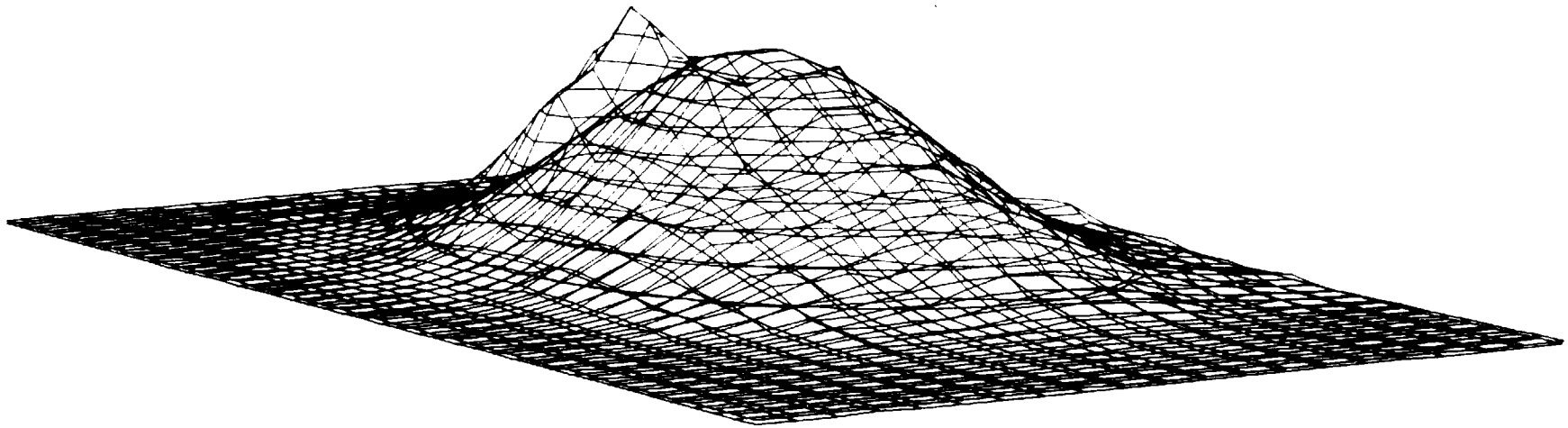

Figure 10C. DRAPER.FIT (Gaussian) for Figure 4A Oriented Clockwise 45 Degrees
Perspective of square field-of-view displayed 21 lines x 42 samples.

3D-PLOT is based on a routine originally prepared by the National Center for Atmospheric Research[4]; however, extensive modifications were made to allow proper handling of the sharp peaks and irregular projection angles which can occur in scanner data. The data points (X, Y, Z, F, where F is the fit) are read in any order from a tape via NTRAN commands, which allows tape positioning under program control. The left margin information is conveyed from the DRAPER.FIT program via the data tape. If both the data and the fit are to be plotted, two colors are used (This two color contrast, unfortunately, does not show in Figures 2-10.)

All inputs are solicited. These include input and output units, scale factor, eye position, focal point and tape positioning instructions. The scale factor is used to convert the Z and F values (still in counts - see explanation of PEAK = in Appendix A) to a visually pleasing size with respect to the X and Y dimensions. To aid in the determination of the scale factor, the PEAK = counts to PK100 kW factor (PKCON) is output by the DRAPER.FIT program. Hence, using PKCON as the scale factor will result in the peaks being one unit high in the Z direction for every kW/cm^2, as compared to X and Y of 21 and 42, respectively. Scalefactor = 10*PKCON was used in Figures 2-10.

VI. SUMMARY

The hardware, software and experience exists to process, interpret and display IR-scanner data. The codes are production oriented, resulting in fast turnaround time with a minimum of tape handling. The slowest portions of the chain shown in Figure 1 are the physical transporting of the tape to and from step 1 (step 1 is presently accomplished at a site remote from BRL) and the delays involved with producing CALCOMP drawings.

[4]*Mr. Thomas Wright, National Center for Atmospheric Research, Boulder, Colorado.*

ACKNOWLEDGEMENT

The authors wish to acknowledge the help of Mr. Earl Weaver, the originator of VLC, and especially Mr. John Kinch, who arranged steps 1, 2 and 3 in the program flow (Figure 1). Mr. Kinch also wrote the machine language programs to unfold the digitized tapes, and rewrote VLC, making it Univac compatible and extending its capabilities.

APPENDIX A

POWER DISTRIBUTION CONTOUR PLOT

The computer printout in Figure A-1 shows a composite frame of beam diagnostic data for a particular test plus relevant frame parameters. The composite frame is generated by summing over the test time the power density in each cell of each frame comprising the composite, normalizing to the (input) total power, and then printed as an array of numbers ranging between 0 and 9 to indicate the contour level of accumulated power in each cell. The following descriptions apply to the hard copy output of the VLC program.

PROJECT: computer storage and user identity code

TEST NO.: device run number

TYPE: target classification; i.e., calorimeter or shield or component 1 or component 2

TIME X.XXX: test time in seconds for the target TYPE (determined from burn wires or high speed photographic measurements). Times are input into the computer code.

XXX FRAMES FROM XXX ON: contour plot data is a composite representing XXX frames of scanner data beginning with frame XXX. The 'start' frame number (also the 'stop' frame number) is obtained from the analog tape record. The start and stop frame numbers are inputs to the computer code.

NOISE IS X COUNTS: Number of noise counts in each cell of those frames used to generate the composite frame. Noise count is determined for each cell from the frames preceeding the 'start' frame and substracted from each cell to remove noise level from the contour data. If noise counts are divided by the number of counts in PEAK = XXXX, signal-to-noise ratio for peak power can be estimated.
Count is defined as the (arbitrary) number of bits of information assigned to the voltage value of the peak power by the digitizing circuitry and is the reference for scaling all power amplitude data.

TOTAL POWER: total test power in kW (as measured by the chopper-detector beam sampler of the device). TOTAL POWER is an input to the computer code.

L AXIS: line axis of 21 rows

S AXIS: sample axis of 42 columns

```
*** U. S. ARMY BALLISTIC RESEARCH LABORATORIES ***
   VULNERABILITY AND LETHALITY DIV.  RAD. ENG. BR.
      DATA REDUCTION DATE: 122776     161031


PROJECT:  EXAMPLE  CASE


 TEST NO. 2102     TYPE:  COMPONENT#1
       TIME 1.000      125 FRAMES FROM   21 ON
    NOISE IS  0 COUNTS.  TOTAL POWER  10.00

                      S   A X I S

      00000000000000000000000000000000000000000000
      00000000000000000001001110000000000000000000
      00000000000000000011012211111100000000000000
      00000000000011111111111101100100000000000000
      00000000011133113211243111001000000000000000
      00000011111111223312321121012210000000000000
      00000000111111132111222331122210000000000000
  L   00001110121112342149625522321000000000000
      00000000111111245S+6444324421111000000000000
  A   00000011100124544565311112221110000000000000
  X   00000011111138B*9324322211110000000000000
  I   00000000112332332574211231111110000000000
  S   00000001111222463122222112111100000000000
      00000000111123211111222211111000000000000
      00000000000001111110111111101000000000000
      00000000000000000001111100000000000000000
      00000000000000000000000000000000000000000
      00000000000000000000000000000000000000000
      00000000000000000000000000000000000000000
      00000000000000000000000000000000000000000
      00000000000000000000000000000000000000000

      +=CENTROID  *=PEAK

FIELD S= 12.70 CM  FIELD L= 12.12 CM
CELL SIZE  S= .302  L= .577  AREA= .1746

COORD          S              L
PEAK       4.838(16)      6.350(11)
CENT       5.978(19)      5.454( 9)
AVGPD        .208
PK100        .972
PK98         .952
PEAK= 14582

CONTUR          0          1          2          3          4          5          6          7          8          9
% PEAK          0          5         20         30         40         50         60         70         80         90
LEVEL        .000       .049       .194       .292       .389       .486       .583       .680       .777       .875
AREA      153.959     48.178     20.074     10.124      5.935      3.317      1.920      1.047       .973       .524
VOLUME                1.000+01   7.000+00   4.673+00   3.321+00   2.181+00   1.467+00   9.125-01   7.031-01   4.967-01
```

Figure A1. Computer Printout - Composite Frame, Beam Diagnostic Data

+ = CENTROID: location of the cell containing the center of mass of the total power

* = PEAK: location of the cell containing the highest accumulation of power density (always a '9' cell)

FIELD: size of the field of view of the scanner shown in the composite frame.

CELL SIZE: 'S' and 'L' dimensions of resolution cell in centimeters and area in cm^2

COORD: coordinates of PEAK and CENT given in linear dimensions and column/row designation with respect to the origin positioned in the upper left-hand corner of the array

AVGPD: average power density of all cells in the array with numbers greater than zero; i.e., the TOTAL POWER divided by AREA of the cells of CONTUR 1

PK100: 100 percent of the peak power density defined as the accumulated power density in the PEAK cell (kW per cm^2)

PK98: 98 percent of the peak power density

PEAK = XXXX: number of counts in the cell containing peak power density

CONTUR 0,1,2,....9: contour intervals corresponding to the contour numbers in the array

% PEAK: minimum value of the percentage of peak power density contained in the contour interval; e.g., for contour 2, all cells of at least 20% of the peak power density but less than 30% are designated as 2 in the array

LEVEL: value of the power density at the beginning of the contour interval designated by % PEAK; e.g., for CONTUR 4 (40%) and PK 100 = 5.00, LEVEL would be $5.00 \times \frac{40}{100} = 2.00$

AREA: area of that portion of the array within the contour designated by CONTUR as well as all higher numbered contours

VOLUME: total power in kW within AREA

APPENDIX B

RADIAL CONDUCTION LIMITS

SPECIAL RESOLUTION REQUIREMENTS FOR HEL BURN DIAGNOSTICS

We assume that damage is thermal.

Rationale: Consider two thermal spikes located a distance 2X apart, each containing energy Q.

$$|\leftarrow X \rightarrow \leftarrow X \rightarrow|$$

$$T_o \qquad T_x$$

If one wishes to resolve these spikes, the diagnostic tool would require spacing between resolution elements of .LT. X. The question is how small is X still meaningful? Our answer: X is certainly meaningless for values smaller than X_o, where X_o is the minimum resolution limit imposed by other causes.

A major contributor to X_o is dictated by radial conduction. A heat conduction equation was employed to determine the temperature difference between T_o and T_x (i.e. $(T_o - T_x)/T_o$, precisely), as a function of X, time, spike to ambient ratio, and thinness and material of plate being irradiated. For these calculations, the following assumptions were made:

(1) the problem could be treated as 1-D. This corresponds to spikes that have a large Y dimension relative to X.

(2) the plate is thermally thin to the beam, and the power is therefore distributed throughout the thinness. (NOTE: The error in this assumption is largely mitigated by the fact that ratios of differences are being taken.) The power in the spike per unit Y is $(I_{SPIKE} - I_{AMB})^*$ THIN, whereas ambient power per unit Y is $I_{AMB}{}^*X$. Hence the ratio of the power in the spike to ambient is

$$(I_{SPIKE} - I_{AMB})^*THIN/I_{AMB}{}^*X = (RATIO-1)^*THIN/X$$

Here, THIN is the thickness of the plate.

Outputs from the computer code are shown in Figures B-1 through B-8. The units are centimeters and seconds, and the diffusivity is appropriate for aluminum. As expected, the importance of the spike decreases with increasing time, and increases with increasing X, RATIO, and plate thickness. Notice, too, that RATIO and THIN are not independent: the curves are actually a function of (RATIO - 1) * THIN/2. Hence Figure B-7 is equivalent to Figure B-4.

DIFFUSIVITY = .900 SPIKE/AMBIENT = 2.00 THINNESS OF PLATE = .254

(TEMP(0,T) - TEMP(L,T))/ TEMP(0,T)

DISTANCE TO BOUNDARY

TIME	*	.200	.400	.600	.800	1.000	1.200	1.400	1.600	1.800	2.000
.050	*	.229	.413	.454	.458	.458	.458	.458	.458	.458	.458
.100	*	.124	.269	.346	.369	.373	.374	.374	.374	.374	.374
.150	*	.085	.194	.275	.311	.324	.327	.328	.328	.328	.329
.200	*	.065	.151	.225	.268	.287	.294	.297	.297	.297	.297
.250	*	.052	.123	.189	.234	.258	.269	.273	.274	.274	.274
.300	*	.044	.104	.162	.207	.234	.247	.253	.255	.256	.257
.350	*	.038	.090	.141	.184	.213	.229	.237	.240	.241	.242
.400	*	.033	.080	.125	.166	.195	.213	.222	.227	.229	.230
.450	*	.030	.071	.113	.151	.180	.198	.209	.215	.218	.219
.500	*	.027	.064	.102	.138	.166	.186	.198	.205	.208	.210

Figure B-1. Ratio of Temperature Difference for .254 cm Aluminum Plate and 2.0 Spike/Ambient Ratio

DIFFUSIVITY = .900 SPIKE/AMBIENT = 3.00 THINNESS OF PLATE = .254

(TEMP(0,T) - TEMP(L,T))/ TEMP(0,T)

DISTANCE TO BOUNDARY

TIME	*	.200	.400	.600	.800	1.000	1.200	1.400	1.600	1.800	2.000
.050	*	.310	.567	.622	.628	.628	.628	.628	.628	.628	.628
.100	*	.173	.391	.503	.536	.543	.545	.545	.545	.545	.545
.150	*	.120	.290	.413	.469	.488	.493	.494	.494	.494	.494
.200	*	.092	.229	.346	.413	.443	.454	.457	.458	.459	.458
.250	*	.074	.189	.295	.367	.405	.421	.428	.430	.431	.431
.300	*	.062	.161	.256	.329	.372	.393	.403	.407	.408	.408
.350	*	.054	.140	.226	.296	.343	.368	.381	.386	.389	.390
.400	*	.047	.124	.202	.269	.317	.346	.361	.369	.372	.373
.450	*	.042	.112	.182	.246	.294	.325	.343	.353	.357	.359
.500	*	.038	.101	.166	.226	.274	.307	.327	.338	.344	.346

Figure B-2. Ratio of Temperature Difference for .254 cm Aluminum Plate and 3.0 Spike/Ambient Ratio

DIFFUSIVITY = .900 SPIKE/AMBIENT = 4.00 THINNESS OF PLATE = .254

(TEMP(0,T) - TEMP(L,T))/ TEMP(0,T)

DISTANCE TO BOUNDARY

TIME	*	.200	.400	.600	.800	1.000	1.200	1.400	1.600	1.800	2.000
.050	*	.350	.647	.710	.717	.717	.717	.717	.717	.717	.717
.100	*	.199	.460	.593	.632	.641	.642	.642	.642	.642	.642
.150	*	.138	.347	.497	.564	.587	.593	.594	.594	.594	.594
.200	*	.106	.277	.422	.504	.541	.554	.558	.559	.559	.559
.250	*	.086	.230	.363	.453	.500	.520	.529	.531	.531	.532
.300	*	.073	.197	.318	.409	.463	.490	.502	.506	.508	.509
.350	*	.063	.172	.282	.372	.430	.462	.478	.485	.488	.489
.400	*	.055	.153	.253	.340	.400	.437	.456	.466	.470	.472
.450	*	.049	.137	.229	.312	.374	.413	.436	.448	.454	.456
.500	*	.044	.125	.210	.288	.350	.392	.417	.431	.439	.442

Figure B-3. Ratio of Temperature Difference for .254 cm Aluminum Plate and 4.0 Spike/Ambient Ratio

DIFFUSIVITY = .900 SPIKE/AMBIENT = 5.00 THINNESS OF PLATE = .254

(TEMP(0,T) - TEMP(L,T))/ TEMP(0,T)

DISTANCE TO BOUNDARY

TIME	*	.200	.400	.600	.800	1.000	1.200	1.400	1.600	1.800	2.000
.050	*	.375	.696	.764	.771	.772	.772	.772	.772	.772	.772
.100	*	.215	.504	.651	.695	.704	.705	.705	.705	.705	.705
.150	*	.150	.385	.553	.628	.653	.660	.661	.661	.661	.661
.200	*	.116	.310	.473	.567	.608	.622	.627	.628	.628	.628
.250	*	.094	.258	.411	.513	.566	.589	.598	.601	.602	.602
.300	*	.079	.222	.361	.466	.528	.558	.572	.577	.579	.580
.350	*	.068	.194	.322	.426	.493	.530	.548	.556	.559	.561
.400	*	.060	.173	.290	.391	.461	.503	.525	.536	.541	.543
.450	*	.054	.156	.264	.360	.432	.478	.504	.518	.525	.528
.500	*	.048	.141	.242	.334	.406	.455	.484	.501	.509	.514

Figure B-4. Ratio of Temperature Difference for .254 cm Aluminum Plate and 5.0 Spike/Ambient Ratio

DIFFUSIVITY = .900 SPIKE/AMBIENT = 10.00 THINNESS OF PLATE = .254

(TEMP(0,T) - TEMP(L,T))/ TEMP(0,T)

DISTANCE TO BOUNDARY

TIME	*	.200	.400	.600	.800	1.000	1.200	1.400	1.600	1.800	2.000
.050	*	.425	.797	.875	.883	.884	.884	.884	.884	.884	.884
.100	*	.248	.602	.779	.831	.841	.843	.843	.843	.843	.843
.150	*	.175	.471	.681	.773	.804	.812	.814	.815	.815	.815
.200	*	.135	.384	.596	.714	.766	.784	.790	.792	.792	.792
.250	*	.110	.324	.526	.659	.727	.756	.768	.771	.773	.773
.300	*	.093	.280	.468	.608	.688	.728	.746	.753	.755	.756
.350	*	.080	.247	.422	.562	.652	.700	.725	.735	.740	.741
.400	*	.071	.220	.383	.521	.617	.673	.703	.718	.725	.728
.450	*	.063	.199	.350	.485	.585	.647	.682	.701	.710	.714
.500	*	.057	.182	.323	.453	.554	.622	.662	.685	.696	.702

Figure B-5. Ratio of Temperature Difference for .254 cm Aluminum Plate and 10.0 Spike/Ambient Ratio

DIFFUSIVITY = .900 SPIKE/AMBIENT = 10.00 THINNESS OF PLATE = .127

(TEMP(0,T) - TEMP(L,T))/ TEMP(0,T)

DISTANCE TO BOUNDARY

TIME	*	.200	.400	.600	.800	1.000	1.200	1.400	1.600	1.800	2.000
.050	*	.384	.714	.784	.792	.792	.792	.792	.792	.792	.792
.100	*	.220	.521	.673	.718	.728	.729	.729	.729	.729	.729
.150	*	.155	.400	.574	.652	.678	.685	.687	.687	.687	.687
.200	*	.119	.322	.494	.591	.634	.649	.654	.655	.655	.656
.250	*	.097	.269	.430	.537	.592	.616	.626	.629	.630	.630
.300	*	.081	.231	.379	.489	.554	.586	.600	.606	.608	.608
.350	*	.070	.203	.338	.447	.518	.557	.576	.585	.588	.589
.400	*	.062	.181	.305	.411	.486	.530	.553	.565	.570	.572
.450	*	.055	.163	.277	.380	.456	.504	.532	.547	.554	.557
.500	*	.050	.148	.254	.352	.429	.481	.512	.529	.538	.543

Figure B-6. Ratio of Temperature Difference for .127 cm Aluminum Plate and 10.0 Spike/Ambient Ratio

DIFFUSIVITY = .900 SPIKE/AMBIENT = 9.00 THINNESS OF PLATE = .127

(TEMP(0,T) - TEMP(L,T))/ TEMP(0,T)

DISTANCE TO BOUNDARY

TIME	*	.200	.400	.600	.800	1.000	1.200	1.400	1.600	1.800	2.000
.050	*	.375	.696	.764	.771	.772	.772	.772	.772	.772	.772
.100	*	.215	.504	.651	.695	.704	.705	.705	.705	.705	.705
.150	*	.150	.385	.553	.628	.653	.660	.661	.661	.661	.661
.200	*	.116	.310	.473	.567	.608	.622	.627	.628	.628	.628
.250	*	.094	.258	.411	.513	.566	.589	.598	.601	.602	.602
.300	*	.079	.222	.361	.466	.528	.558	.572	.577	.579	.580
.350	*	.068	.194	.322	.426	.493	.530	.548	.556	.559	.561
.400	*	.060	.173	.290	.391	.461	.503	.525	.536	.541	.543
.450	*	.054	.156	.264	.360	.432	.478	.504	.518	.525	.528
.500	*	.048	.141	.242	.334	.406	.455	.484	.501	.509	.514

Figure B-7. Ratio of Temperature Difference for .127 cm Aluminum Plate and 9.0 Spike/Ambient Ratio

DIFFUSIVITY = .900 SPIKE/AMBIENT = 3.00 THINNESS OF PLATE = .127

(TEMP(0,T) - TEMP(L,T))/ TEMP(0,T)

		DISTANCE TO BOUNDARY									
TIME	*	.200	.400	.600	.800	1.000	1.200	1.400	1.600	1.800	2.000
.050	*	.229	.413	.454	.458	.458	.458	.458	.458	.458	.458
.100	*	.124	.269	.346	.369	.373	.374	.374	.374	.374	.374
.150	*	.085	.194	.275	.311	.324	.327	.328	.328	.328	.328
.200	*	.065	.151	.225	.268	.287	.294	.297	.297	.297	.297
.250	*	.052	.123	.189	.234	.258	.269	.273	.274	.274	.274
.300	*	.044	.104	.162	.207	.234	.247	.253	.255	.256	.257
.350	*	.038	.090	.141	.184	.213	.229	.237	.240	.241	.242
.400	*	.033	.080	.125	.166	.195	.213	.222	.227	.229	.230
.450	*	.030	.071	.113	.151	.180	.198	.209	.215	.218	.219
.500	*	.027	.064	.102	.138	.166	.186	.198	.205	.208	.210

Figure B-8. Ratio of Temperature Difference for .127 cm Aluminum Plate and 3.0 Spike/Ambient Ratio

It remains to apply these results to the question of beam diagnostics. A 0.127 cm (50 mil) sheet is an average shield. Consider an average flux of 3 kW/cm^2, with spikes as high as 9 kW/cm^2. Burn through should take in the order of 0.10 second. Error in the time measurement is probably ∿20%. Figure B-8 gives a 20% temperature difference at 0.4 cm. Hence, it makes no sense to sample more closely than that. A more significant difference occurs at 0.6 cm. At 0.5 cm for X, the ratio of power in the spikes to ambient is 0.5, which is quite pathelogical (hefty spikes!). It therefore appears that 0.5 cm is a lower limit on the reasonable resolution at the target.

The following descriptions apply to the hard copy outputs of the computer code for temperature difference in Figures B-1 through B-8:

DIFFUSIVITY = X.XXX	rate of diffusion of aluminum plate
SPIKE/AMBIENT = X.XX	ratio of power in the spike to ambient power per unit Y
THINNESS OF PLATE = X.XXX	thickness of plate (aluminum) in cm
TEMP (0,T)	temperature at spike at time T
TEMP (L, T)	temperature between spikes at Time T
TIME	.050 to .500 sec at dt = .050 sec
DISTANCE TO BOUNDARY	.200 to 2.000 cm at 0.2 cm intervals

APPENDIX C

DRAPER.FIT

The composite frame data, as shown on the contour plots (reference Appendix A), is smoothed to reflect the resolution limits imposed by radial conduction. It is then fit by an equivalent Gaussian of the form

$$I(x,y) = I_o * \exp\left(-(x-x_o)^2/2\sigma_x^2\right) * \exp\left(-(y-y_o)^2/2\sigma_y^2\right) + C$$

Here x_o and y_o are the energy distribution centroid, σ_x and σ_y the standard deviation of the distribution, and I_o is the Equivalent Gaussian intensity. C is the baseline. This intensity is derived either from an I^2 integration based on an intensity criterion appearing in a report by the Charles Stark Draper Company or on total power. The following descriptions apply to the hard copy output of the DRAPER.FIT program shown in Figure C-1.

***RUN NUMBER XXXX: device run number

TOTAL POWER XXX.XX: total test power in kW (measured by the chopper-detector beam sampler of the device)

NOISE X: number noise counts per cell

X TIME INTERVALS...X.XXX X.XXX: no. of time intervals for the run number with duration of time intervals in seconds

FIT # XX: sequence number assigned by the Draper program for either POWER or DRAPER.FIT

CHI SQ. = X.XXX: results of chi-square test fitting the composite frame contour data against the Gaussian distribution by DRAPER program

PKCON = X.XXX-XX: conversion factor is ratio of PK100 to PEAK = used to convert the Z scale of the 3D-PLOT program to compatible range with respect to the S and L axes.

(The following information also appears on 3D-PLOT Calcomp plots)

RUN NO. XXXX.X: run number and time sequence number assigned to FIT # above

ON TIME X.XX: test time in seconds

TP XXX.X: total test power in kW

```
*** RUN NUMBER 2102   TOTAL POWER =  10.00    NOISE =  0
 1 TIME INTERVALS ...  1.000
POWER FIT #    1  CHI SQ. =    .644       PKCON =   6.664-05

RUN NO. 2102.1  ON TIME 1.00  TP  10.0  N 0 ( 9.4, 19.8)  1.8,  1.8    .481    .006
```

Figure C1. Computer Printout - DRAPER.FIT Program

N X: number of noise counts in RUN NO. above

(XX.X, XX.X): L and S coordinates of the peak value of the Gaussian fit

X.X,X.X: standard deviation of Gaussian fit in L and S directions in cm

X.XXX: peak value of the Gaussian fit in kW cm^{-2}

.XXX: baseline of Gaussian fit in $kWcm^{-2}$

DISTRIBUTION LIST

No. of Copies	Organization
12	Commander Defense Documentation Center ATTN: DDC-TCA Cameron Station Alexandria, VA 22314
1	Director of Defense Research and Engineering ATTN: Asst Dir (Space & Advanced System) The Pentagon Washington, DC 20301
1	Defense Advanced Research Projects Agency ATTN: Dir, Laser Div 1400 Wilson Boulevard Arlington, VA 22209
2	Director Institute for Defense Analysis ATTN: Classified Library Dr. R. G. Finke Dr. J. Ross 400 Army Navy Drive Arlington, VA 22202
1	Commander US Army Materiel Development and Readiness Command ATTN: DRCDMA-ST 5001 Eisenhower Avenue Alexandria, VA 22333
1	Commander US Army Aviation Systems Command ATTN: DRSAV-E 12th and Spruce Streets St. Louis, MO 63166
1	Director US Army Mobility Research and Development Laboratory Ames Research Center Moffett Field, CA 94035
1	Director US Army Air Mobility Research and Development Laboratory ATTN: SAVDL-EU-MOS, E.Gilbert Fort Eustis, VA 23604
1	Commander US Army Electronics Command ATTN: DRSEL-RD Fort Monmouth, NJ 07703
1	Commander US Army Missile Research and Development Command ATTN: DRDMI-R Redstone Arsenal, AL 35809
6	Commander US Army Missile Research and Development Command ATTN: High Energy Laser Project, DRCPM-HEL Redstone Arsenal, AL 35809
3	Commander US Army Missile Research and Development Command High Energy Laser Directorate ATTN: DRSMI-RHS, Dr. R. Conrad DRSMI-RHAE, A. Jenkins DRSMI-RH, W. Gurley Redstone Arsenal, AL 35809
1	Commander US Army Tank Automotive Development Command ATTN: DRDTA-RWL Warren, MI 48090
2	Commander US Army Mobility Equipment Research & Development Command ATTN: Tech Docu Cen, Bldg. 315 DRSME-RZT Fort Belvoir, VA 22060

DISTRIBUTION LIST

No. of Copies	Organization
1	Commander US Army Armament Materiel Readiness Command Rock Island, IL 61202
1	Director US Army Frankford Arsenal Pittman-Dunn Research Lab ATTN: SARFA-L5000, Dr. Holtz Philadelphia, PA 19137
1	Commander US Army Rock Island Arsenal ATTN: SARRI-LR, J.W.McGarvey Rock Island, IL 61202
1	Commander US Army Harry Diamond Labs ATTN: DRXDO-TI 2800 Powder Mill Road Adelphi, MD 20783
2	Director US Army Materials and Mechanics Research Center ATTN: DRXMR-HW, S. Arnold R. Fitzpatrick Watertown, MA 02172
1	Director US Army TRADOC Systems Analysis Activity ATTN: ATAA-SA White Sands Missile Range NM 88002
2	HQDA (DAMA-WSN-T, Pellegrini; DAMA-WS, McCorkle) Washington, DC 20310
2	HQDA (DAMA-AR, Garker; DAMA-RAA, LTC Narus) Washington, DC 20310
2	Director US Army Advanced BMD Technology Center ATTN: ATC-O ATC-T, J.Hagefstration P. O. Box 1500 Huntsville, AL 35807
1	Commander US Naval Air Systems Command ATTN: AIR-530313, R. Hume AIR-5204, LTC R. Remers Washington, DC 20361
2	Commander US Naval Ordnance Sys Command ATTN: CPT Skolnik, PMO-405 Mr. L. Stoessel, PMS-405 Washington, DC 20360
1	Commander US Naval Surface Weapons Center ATTN: Code DG13, J. Bland Dahlgren, VA 22448
2	Commander US Naval Surface Weapons Center ATTN: Code 413, R. Culpepper Code 433, F. Cooke Silver Spring, MD 20910
4	Director US Naval Weapons Center ATTN: Code 4011, E.B. Niccum Code 4011, H. Jeffers Code 4565, C. Sandberg Code 4011, W. McCanless China Lake, CA 93555
3	Commander US Naval Research Laboratory ATTN: Code 6330, A. Schindler Code 6332, T. Schriempf Code 6425, Dr. Wenzel Washington, DC 20375

DISTRIBUTION LIST

No. of Copies	Organization
2	Superintendent US Naval Postgraduate School ATTN: Dept of Physics and Chemistry, Prof J.R.Neighbours Library, Code 2124 Monterey, CA 93940
1	RADC/OCSE, Mr. R. Urtz Griffiss AFB, NY 13441
7	AFWL (COL D. Lamberson; Dr. Rudder; MAJ H. Rede; LTC K. Gilbert; MAJ W. Godsey; CPT J. Jackson; CPT D.Evans) Kirtland AFB, NM 87117
1	AFAPL/SFH, Mr. A. Ferrenberg Wright-Patterson AFB, OH 45433
1	AFFDL/FEN, CPT G. Camburn Wright-Patterson AFB, OH 45433
3	AFML (LPJ, MAJ P. Elder; LC, Mr. G. Denman; MBC, Mr. R. Farmer) Wright-Patterson AFB, OH 45433
1	ASD/ENFTV, D. Wallick Wright-Patterson AFB, OH 45433
1	Director Lawrence Livermore Laboratory ATTN: Dr. J. Fleck, L-71 (Mail Code) P. O. Box 808 Livermore, CA 94550
1	Director Lawrence Livermore Laboratory ATTN: Dr. J. Emmett, L-555 (Mail Code) P. O. Box 808 Livermore, CA 94550
1	Director Lawrence Livermore Laboratory ATTN: Dr. H. Kruger P. O. Box 808 Livermore, CA 94550
1	AVCO/Lycoming ATTN: Mr. Richard Cuny 550 Main Street Stratford, CT 08497
1	Bell Helicopter Textron ATTN: Mr. J. R. Johnson P. O. Box 482 Fort Worth, TX 76101
1	Boeing Vertol Division ATTN: Mr. Joseph Gonsalves P. O. Box 16858 Philadelphia, PA 19142
2	The Boeing Company Aerospace Group ATTN: Mr. R. Blaisdell Mr. H. Brettman P. O. Box 3999 Seattle, WA 98124
1	Falcon R&D Company ATTN: Ms. L. Doran 601 San Pedro, NE Albuquerque, NM 87108
2	General Electric Company ATTN: Mr. Winter, Room 2534 Mr. D. Rich 3198 Chestnut Street Philadelphia, PA 19101
1	General Electric Company ATTN: Mr. Edward Richardson 1000 Western Avenue W. Lynn, MA 01910

DISTRIBUTION LIST

No. of Copies	Organization
1	General Electric Company Valley Forge Space Center ATTN: Mr. W. J. East P. O. Box 8555 Philadelphia, PA 19101
1	General Research Corporation ATTN: Dr. G.K. Warmbrod 307 Wynn Drive Huntsville, AL 35807
1	McDonnell Douglas Astronautics Company ATTN: Dr. W. Bozich 5301 Bolsa Avenue Huntington Beach, CA 92647
2	McDonnell Douglas Corporation ATTN: Dr. T. Ender Mr. E. Wiggins P. O. Box 516 St. Louis, MO 63166
1	Mitre Corporation ATTN: Mr. N. Harmon P. O. Box 208 Bedford, MA 01730
1	Lockheed Missile and Space Company, HREC ATTN: Mr. Bill Hendricks 4800 Bradford Drive Huntsville, AL 35807
1	Northrup Research and Technology Center ATTN: C. S. Steinberg 3401 W. Broadway Hawthorne, CA 90250
1	Pratt & Whitney Aircraft Florida R&D Center ATTN: Mr. James DeLonga Bee Line Highway W. Palm Beach, FL 33401
1	Quest Research Corporation ATTN: Mr. John P. Alcott Suite 407, 6845 Elm Street McLean, VA 22101
2	R&D Associates ATTN: Dr. R. Hundley Mr. D. Gakenheimer P. O. Box 9695 Marina del Rey, CA 90291
1	Science Applications, Inc. ATTN: Dr. R. Meredith P. O. Box 328 Ann Arbor, MI 48103
2	Science Applications, Inc. ATTN: Dr. Peckham Dr. E. Alcarez 2361 Jefferson Davis Highway Arlington, VA 22202
1	Science Applications, Inc. ATTN: Richard Wade 2028 Powers Ferry Road Suite 260 Atlanta, GA 30339
1	Science Applications, Inc. ATTN: Dr. J. Asmus P. O. Box 2351 La Jolla, CA 92037
1	Sikorsky Aircraft Division ATTN: Mr. James Foulk North Main Stratford, CT 06602
1	TRW Systems Group ATTN: Mr. Fred Knopf 7702 Governors Drive West Huntsville, AL 35805

DISTRIBUTION LIST

No. of Copies	Organization
2	United Aircraft Research Lab ATTN: Mr. G. McLafferty Mr. A. Angelbeek 400 Main Street East Hartford, CT 06108
1	Vought Corporation ATTN: Mr. B. Forcht P. O. Box 5907 Dallas, TX 75222
2	Battelle Memorial Institute Columbus Laboratory ATTN: Mr. K. Wilkes Mr. S. Rubin 505 King Avenue Columbus, OH 43201
4	Massachusetts Institute of Technology, Lincoln Lab ATTN: Dr. Marquet Dr. Rediker Dr. Edelberg Dr. Reis P. O. Box 73 Lexington, MA 02173
1	Stanford Research Institute ATTN: Dr. R. Armistead Menlo Park, CA 94025
1	Stanford Research Institute ATTN: Mr. John H. Hennings 306 Wynn Drive, NW Huntsville, AL 35805
	Aberdeen Proving Ground
	Dir, USAMSAA ATTN: DRXSY, Dr. Sperrazza DRXSY-AFF, Mr. D.Smith Mr. A. Henderson Marine Corps Ln Ofc